REFERENCES

Allen, J.R.L. (1971). Bed forms due to mass transfer in turbulent flows: a kaleidoscope of phenomena. Journal of Fluid Mechanics, 49(1), 49-63.

Allen, J.R.L. (1971). Transverse erosional marks of mud and rock: their physical basis and geological significance. Sedimentary Geology, 5, 167-385.

Azimi, A., Papangelakis, V.G. and Dutrizac, J.E. (2007). Modelling of calcium sulphate solubility in concentrated multi-component sulphate solutions. Fluid Phase Equilibria, 260, 300-315.

Berger, F.P. and Hau, K. -F. F. -L. (1977). Mass transfer in turbulent pipe flow measured by the electrochemical method. Journal of Heat Mass Transfer, 20, 1185-1194

Blumberg, P.N. (1970). Flutes: a study of stable, periodic dissolution profiles resulting from the interaction of a soluble surface and an adjacent turbulent flow. PhD thesis, University of Michigan.

Blumberg, P.N. and Curl R.L. (1974). Experimental and theoretical studies of dissolution roughness. Journal of Fluid Mechanics, 65(4), 735-751.

Burrill, K.A. and Cheluget E.L. (1998). Corrosion of CANDU outlet feeder pipes. Paper presented at the 1998 JAIF International Conference, Japan Atomic Industrial Forum on Water Chemistry in Nuclear Power Plants, October 13-16. Kashiwazaki, Japan.

Coney, M.W.E., Wilkin, S.J. and Oates, H.S. (1982). Thermal-hydraulic effects on mass transfer behaviour and on erosion-corrosion metal loss rates. EdF (International Specialists' Meeting on Erosion-Corrosion of steels in high temperature water and wet steam, France.

Curl, R.L. (1974). Deducing flow velocity in cave conduits from scallops. The NSS Bulletin, 36(2), 1-5.

Ferng Y., Yin-Pang MA. And Kuo-Tong MA. (1999). Flow-assisted corrosion of pipes. Nuclear Technology, 126

Henderson, E.P. and Perry, S.H., (1958). Studies on siderites. Proc.U.S. Natl. Museum, 107, 339-403.

James, A.N. and Lupton, A.R.R., (1978). Gypsum and anhydrite in foundations of hydraulic structures. Geotechique, 28(3), 249-272.

Jeschke, A.A., Vosbeck, K. and Dreybrodt, W. (2001). Surface controlled dissolution rates of gypsum in aqueous solutions exhibit non linear dissolution kinetics. Geochimica et Cosmochimica Acta, 65(1), 27-34.

Lebedev, A.L. and Lekhov, A.V. (1989). Dissolution kinetics of natural-gypsum in water at 5-25oC. Moscow University. 6:865-874.

Leighly, J., (1948). Cuspate surfaces of melting ice and firn. Geograph. Rev., 38:300-306.

Lertsurasakda, C. (2007). The effect of surface scalloping on flow hydrodynamics and pressure drop. M.S. Thesis, The Petroleum and Petrochemical College, Chulalongkorn University.

Lister, D.H., Gauthier, P., Goszczynski, J. and Slade, J., (1998). The accelerated corrosion of CANDU primary piping. Paper presented at the 1998 JAIF International Conference, Japan Atomic Industrial Forum on Water Chemistry in Nuclear Power Plants, Sept 7-11.

Liu, S. and Nancollas, G.H., (1971). The kinetics of dissolution of calcium sulfate dehydrate. Journal of Inorganic Nuclear Chemistry, 33, 2311-2316.

Marshall, L.W. and Slusher, R., (1975) The ionization constant of nitric acid at high temperatures from solubilities of calcium sulfate in HNO3-H2O, 100-350°C; activity coefficients and thermodynamic functions. Journal of Inorganic Nuclear Chemistry, 37, 1191-1202.

Opdyke, N.B., Gust, G. and Ledwell, R.J. (1987) Mass transfer from smooth alabaster surfaces in turbulent flows. Geophysical research letters, 14(11), 1131-1134.

Perry H.R. and Green W.D. (1997) Perry's Chemical Engineers' Handbook: Seventh Edition. New York: McGraw-Hill.

Raines, M. and Dewers, T., (1997) Mixed kinetics control of fluid-rock interaction in reservoir production scenarios. Journal of Petroleum Science and Engineering, 17, 139-155.

Rechenberg, W. and Sprung, S., (1983) Composition of the solution in the hydration of cement. Cement and Concrete Research, 13, 119-126.

Shao, Y. (2006) The scalloping phenomenon and the influence of oxygen on flow-accelerated corrosion in feedwater systems. Master of science in engineering thesis, University of New Brunswick.

Sharp, J.P., (1974) The wolf-creek glaciers, St Elias Range, Yukon Territory. Geograph. Rev., 37, 26-52.

Villien, B., Zheng, Y. and Lister D.H. (2001) The scalloping phenomenon and its significance in flow assisted-corrosion. Proceedings of the twenty sixth annual CNS-CAN student conference, Toronto (June).

Villien, B., Zheng, Y. and Lister D.H. (2005) Surface dissolution and the development of scallops. Chem. Eng. Comm., 192, 125-136.

APPENDICES

Appendix A Dissolution Rate

The effluent, from the test section, was collected every 30 minutes and it was analyzed with AAS for the calcium concentration. The samples were diluted 20 times to fit AAS limitation. Scallop characteristics were obtained by taking photos every 30 minutes. Thickness of plaster pipe was measured every centimeter along the pipe and calculated to get the dissolution rate profile along the pipe at the end of the test. Moreover, pressure drop was also measured every 30 minutes between the inlet and outlet of the conduit by pressure transducer.

A.1 Dissolution Rate with Time

A.1.1 Effect of Flow Rate

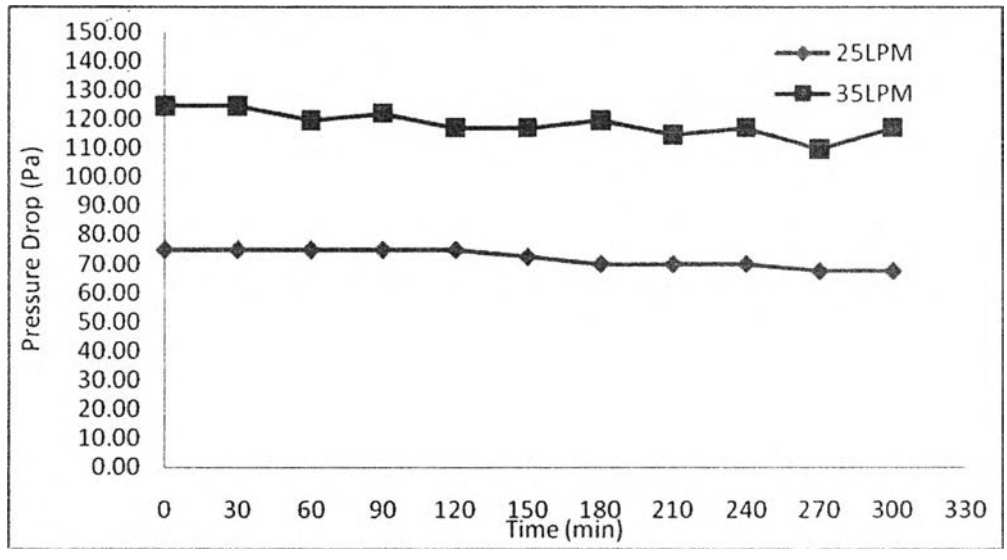

Figure A.1 Dissolution rate with time at pH7 and 30°C.

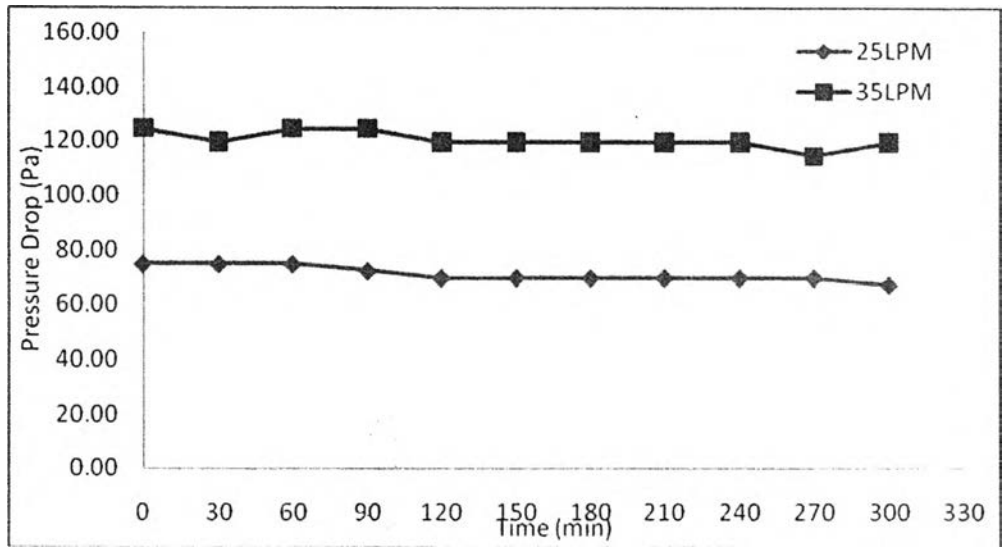

Figure A.2 Dissolution rate with time at pH10 and 30°C.

A.1.2 Effect of Defect Size

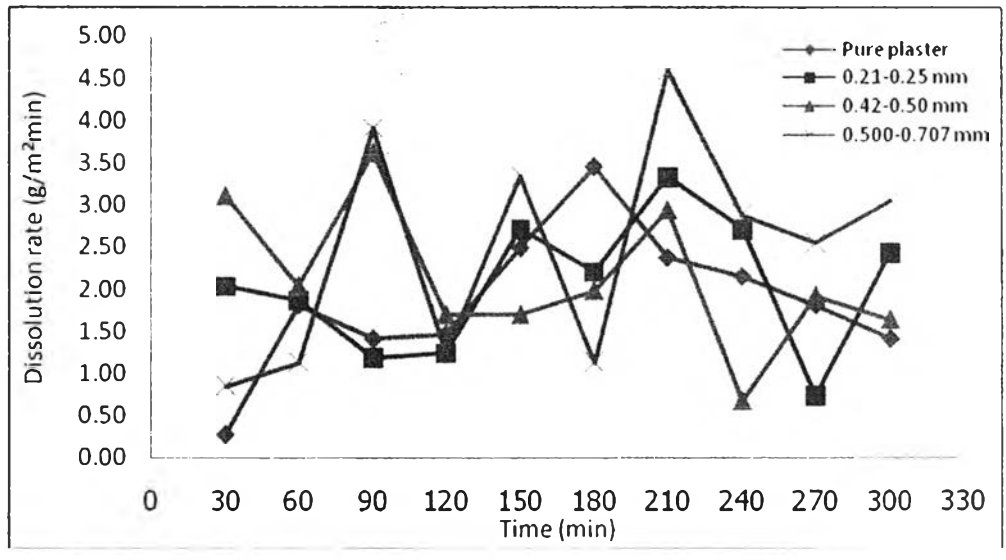

Figure A.3 Dissolution rate with time at different sizes of particles, 25°C, 100 defects/cm^3 and 25LPM.

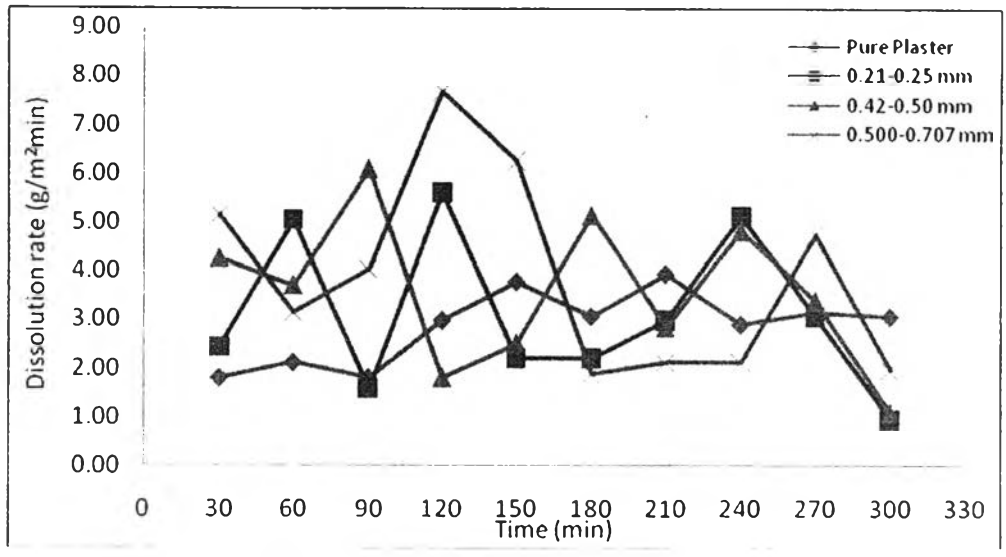

Figure A.4 Dissolution rate with time at different sizes of particles, 25°C, 100 defects/cm^3 and 35LPM.

Table A.1 Average dissolution rate calculating from AAS at different sizes of initial defects and 25 LPM.

t (min)	Pure Plaster	0.21-0.25 mm 100 defects/cm^3	0.42-0.50 mm 100 defects/cm^3	0.500-0.707 mm 100 defects/cm^3
30	0.283	2.036	3.111	0.848
60	1.810	1.867	2.036	1.131
90	1.414	1.188	3.620	3.903
120	1.471	1.244	1.697	1.244
150	2.489	2.715	1.697	3.337
180	3.451	2.206	1.980	1.131
210	2.376	3.337	2.941	4.582
240	2.149	2.715	0.679	2.885
270	1.810	0.735	1.923	2.545
300	1.414	2.432	1.640	3.055
Average dissolution rate (g/m^{2}min)	1.867	2.048	2.133	2.466

Table A.2 Average dissolution rate calculating from AAS at different sizes of initial defects and 35 LPM.

t (min)	Pure Plaster	0.21-0.25 mm 100 defects/cm^3	0.42-0.50 mm 100 defects/cm^3	0.500-0.707 mm 100 defects/cm^3
30	1.821	2.455	4.276	5.147
60	2.138	5.068	3.722	3.168
90	1.821	1.584	6.098	4.039
120	3.009	5.623	1.821	7.682
150	3.801	2.217	2.534	6.256
180	3.088	2.217	5.147	1.901
210	3.960	3.009	2.851	2.138
240	2.930	5.147	4.831	2.138
270	3.168	3.088	3.405	4.752
300	3.088	0.950	1.109	1.980
Average dissolution rate ($g/in^2 min$)	2.882	3.136	3.579	3.920

A.1.3 Effect of Defect Concentration

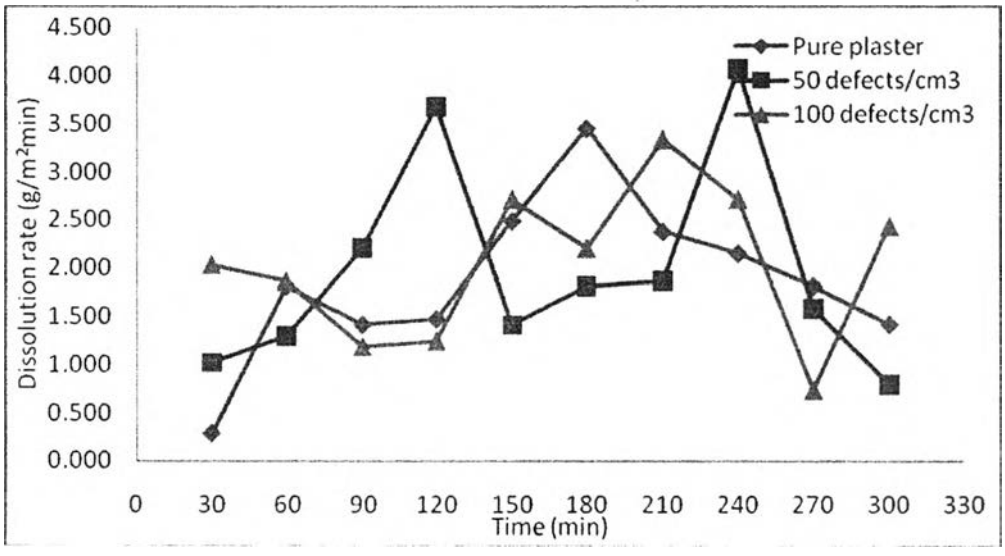

Figure A.5 Dissolution rate with time at different concentrations of particles, 0.21-0.25 mm, 25°C and 25LPM.

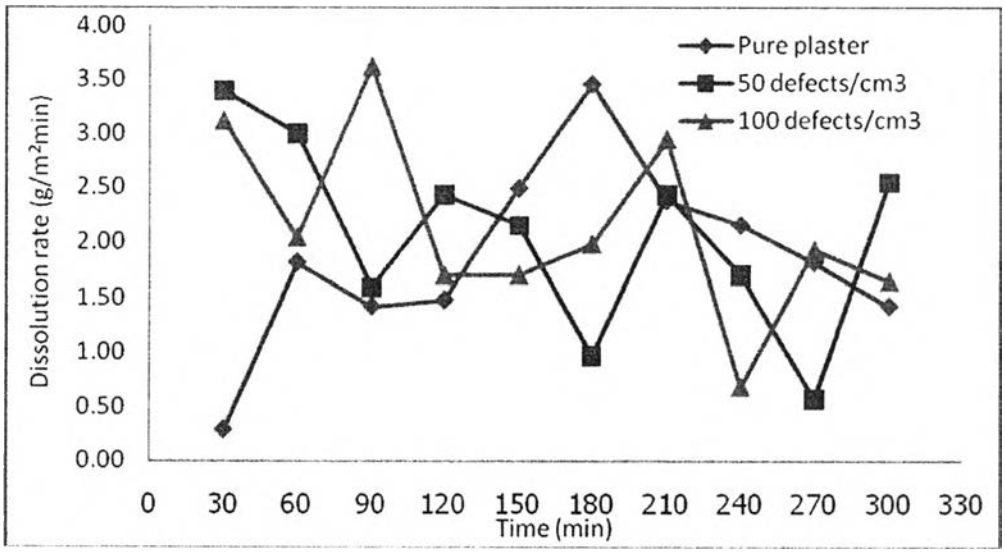

Figure A.6 Dissolution rate with time at different concentrations of particles, 0.42-0.50 mm, 25°C and 25LPM.

Table A.3 Average dissolution rate calculating from AAS at different concentrations of initial defects at defect size of 0.21-0.25 mm and 25LPM.

t(min)	Pure Plaster	0.21-0.25 mm 50 defects/cm^3	0.21-0.25 mm 100 defects/cm^3
30	0.283	1.018	2.036
60	1.810	1.301	1.867
90	1.414	2.206	1.188
120	1.471	3.677	1.244
150	2.489	1.414	2.715
180	3.451	1.810	2.206
210	2.376	1.867	3.337
240	2.149	4.073	2.715
270	1.810	1.584	0.735
300	1.414	0.792	2.432
Average dissolution rate (g/m^2min)	1.867	1.974	2.048

Table A.4 Average dissolution rate calculating from AAS at different concentrations of initial defects at defect size of 0.42-0.50 mm and 25LPM.

t(min)	Pure Plaster	0.42-0.50 mm 50 defects/cm^3	0.42-0.50 mm 100 defects/cm^3
30	0.283	3.394	3.111
60	1.810	2.998	2.036
90	1.414	1.584	3.620
120	1.471	2.432	1.697
150	2.489	2.149	1.697
180	3.451	0.962	1.980
210	2.376	2.432	2.941
240	2.149	1.697	0.679
270	1.810	0.566	1.923
300	1.414	2.545	1.640
Average dissolution rate (g/m^{2}min)	1.867	2.076	2.133

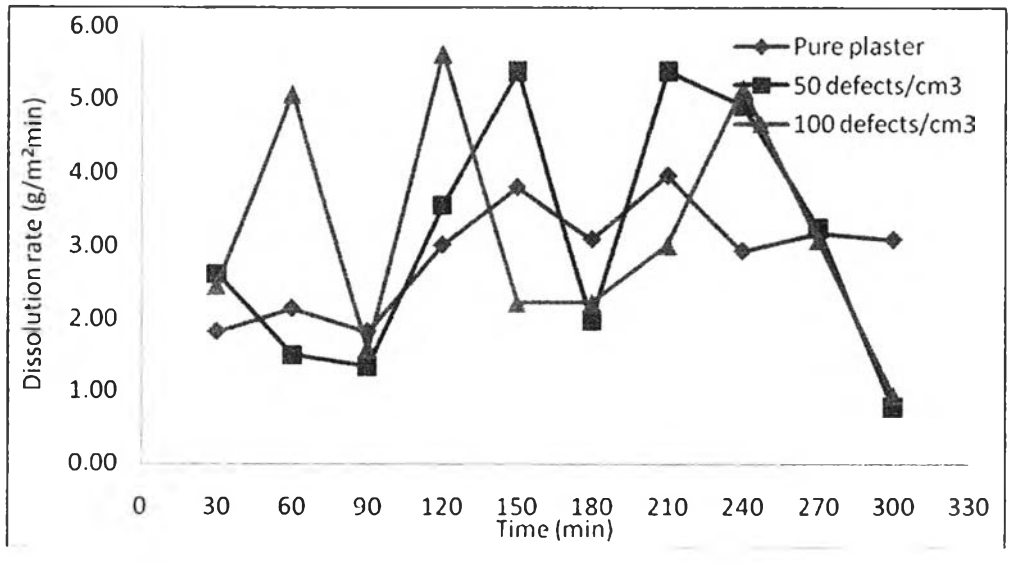

Figure A.7 Dissolution rate with time at different concentrations of particles, 0.21-0.25 mm, 25°C and 35LPM.

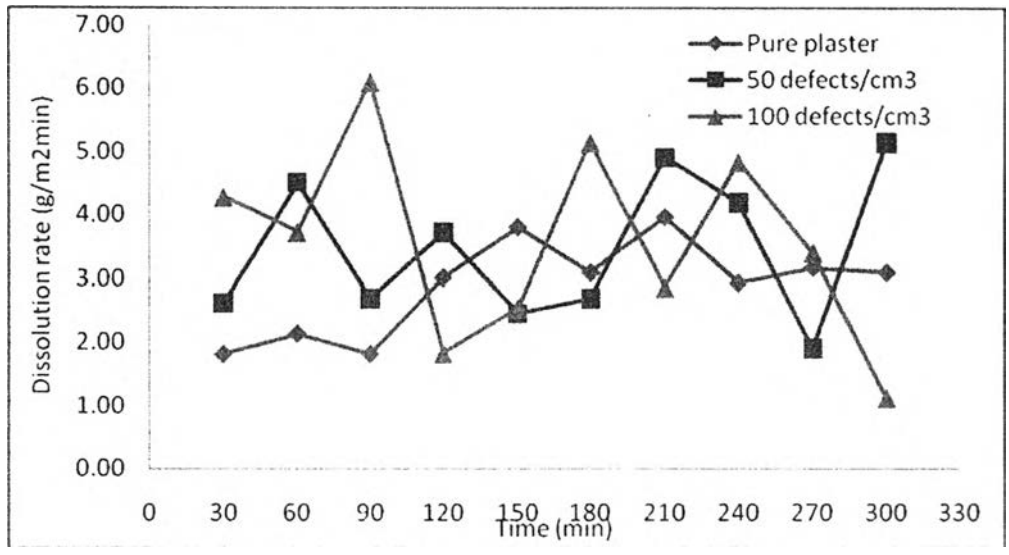

Figure A.8 Dissolution rate with time at different concentrations of particles, 0.42-0.50 mm, 25°C and 35LPM.

Table A.5 Average dissolution rate calculating from AAS at different concentrations of initial defects at defect size of 0.21-0.25 mm and 35LPM.

t (min)	Pure Plaster	0.21-0.25 mm 50 defects/cm^3	0.21-0.25 mm 100 defects/cm^3
30	1.821	2.613	2.455
60	2.138	1.505	5.068
90	1.821	1.346	1.584
120	3.009	3.564	5.623
150	3.801	5.385	2.217
180	3.088	1.980	2.217
210	3.960	5.385	3.009
240	2.930	4.910	5.147
270	3.168	3.247	3.088
300	3.088	0.792	0.950
Average dissolution rate (g/m^{2}min)	2.883	3.136	3.136

Table A.6 Average dissolution rate calculating from AAS at different concentrations of initial defects at defect size of 0.42-0.50 mm and 35LPM.

t (min)	Pure Plaster	0.42-0.50 mm 50 defects/cm^3	0.42-0.50 mm 100 defects/cm^3
30	1.821	2.613	4.276
60	2.138	4.514	3.722
90	1.821	2.693	6.098
120	3.009	3.722	1.821
150	3.801	2.455	2.534
180	3.088	2.693	5.147
210	3.960	4.910	2.851
240	2.930	4.197	4.831
270	3.168	1.901	3.405
300	3.088	5.147	1.109
Average dissolution rate (g/m^2min)	2.883	3.484	3.579

A.1.4 Effect of Temperature

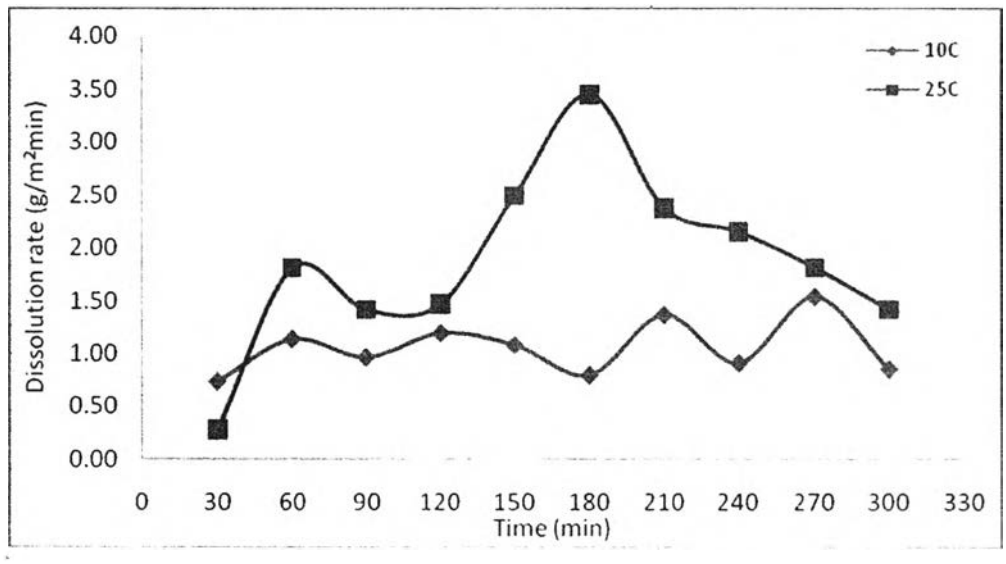

Figure A.9 Dissolution rate with time at different temperatures, pure plaster and 25LPM.

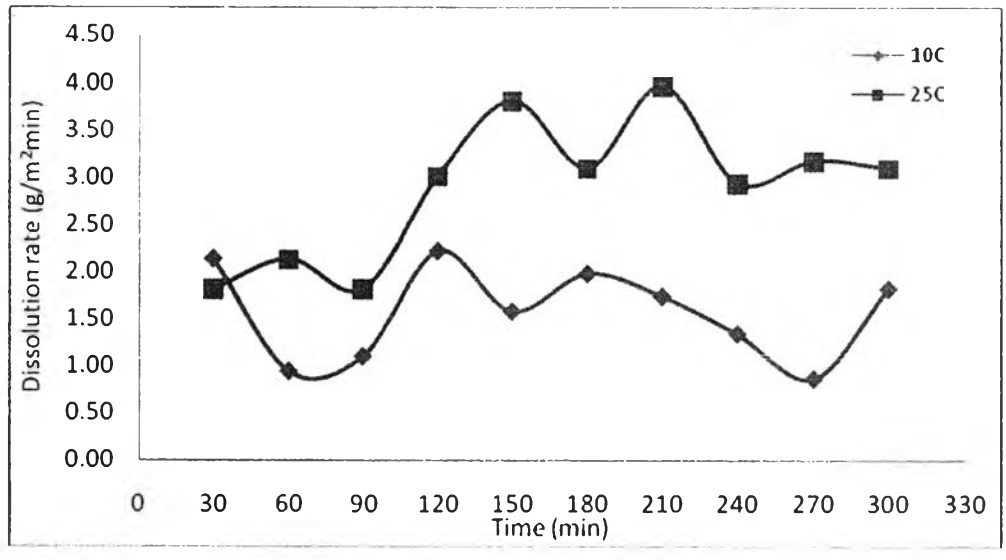

Figure A.10 Dissolution rate with time at different temperatures, pure plaster and 35LPM.

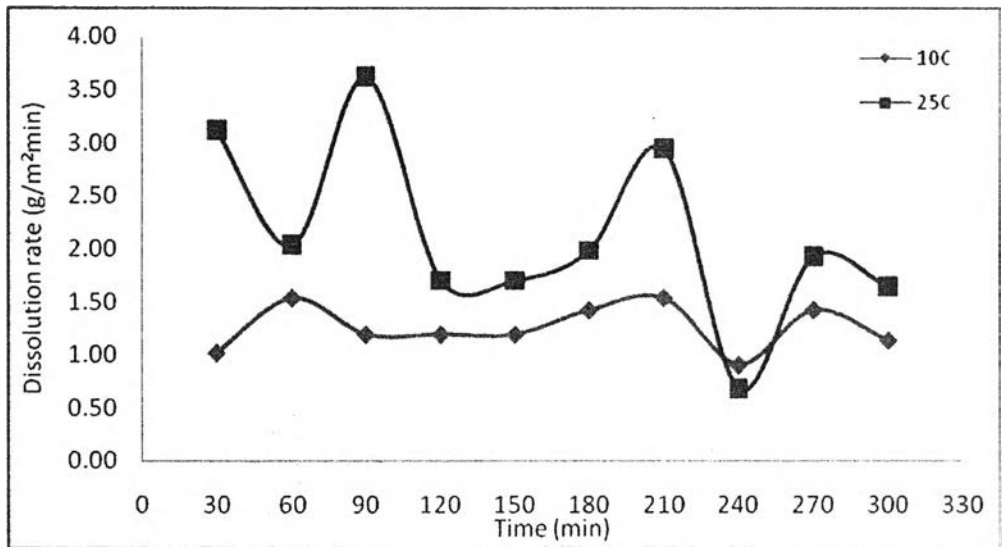

Figure A.11 Dissolution rate with time at different temperatures, 0.42-0.50 mm, 50 defects/cm^3 and 25LPM.

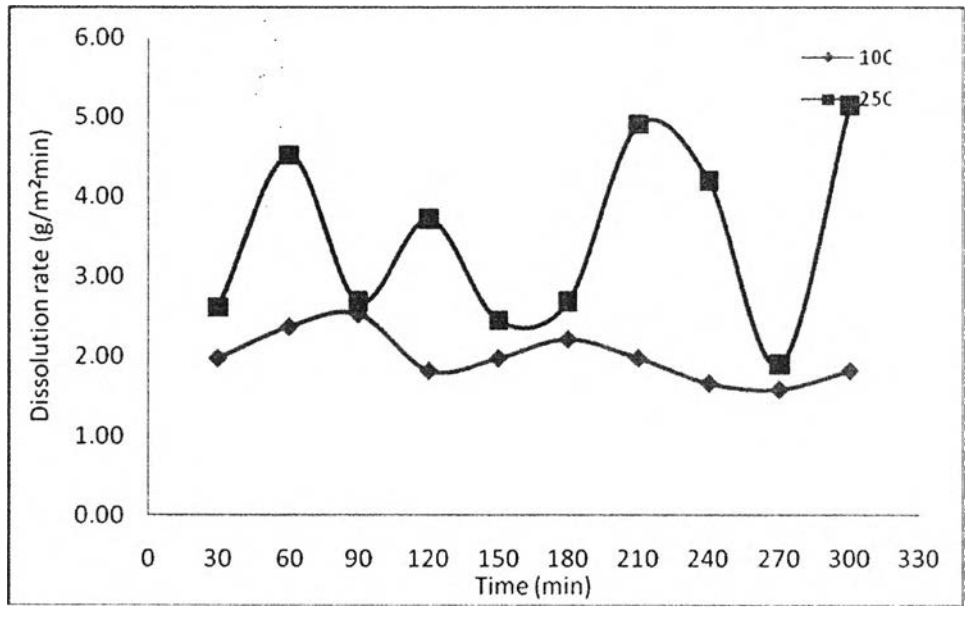

Figure A.12 Dissolution rate with time at different temperatures, 0.42-0.50 mm, 50 defects/cm^3 and 35LPM.

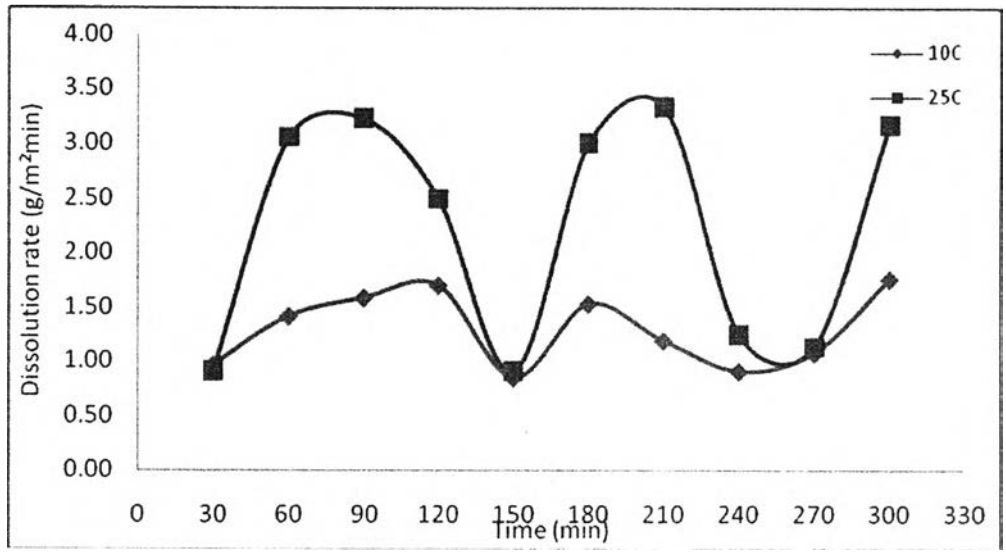

Figure A.13 Dissolution rate with time at different temperatures, 0.500-0.707 mm, 50defects/cm^3 and 25LPM.

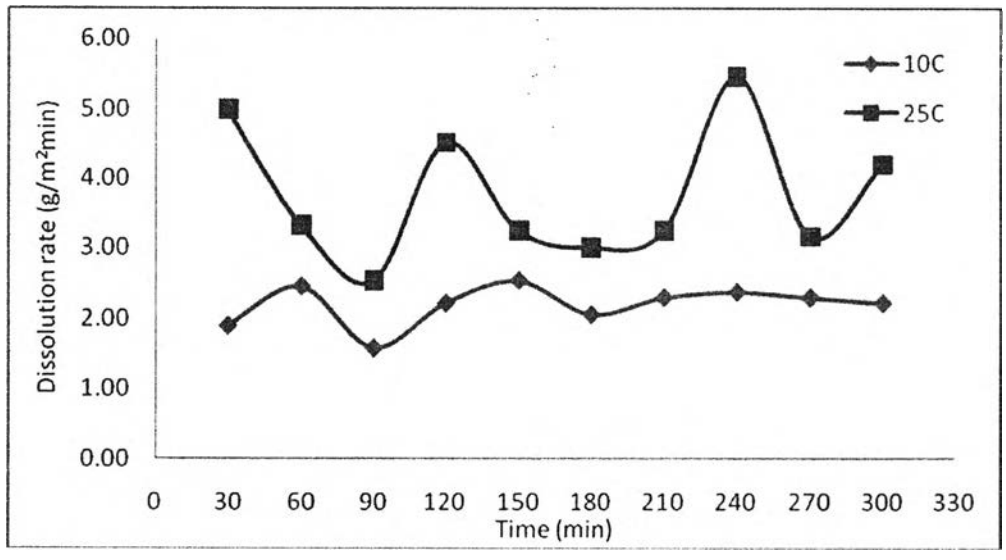

Figure A.14 Dissolution rate with time at different temperatures, 0.500-0.707 mm, 50 defects/cm^3 and 35LPM.

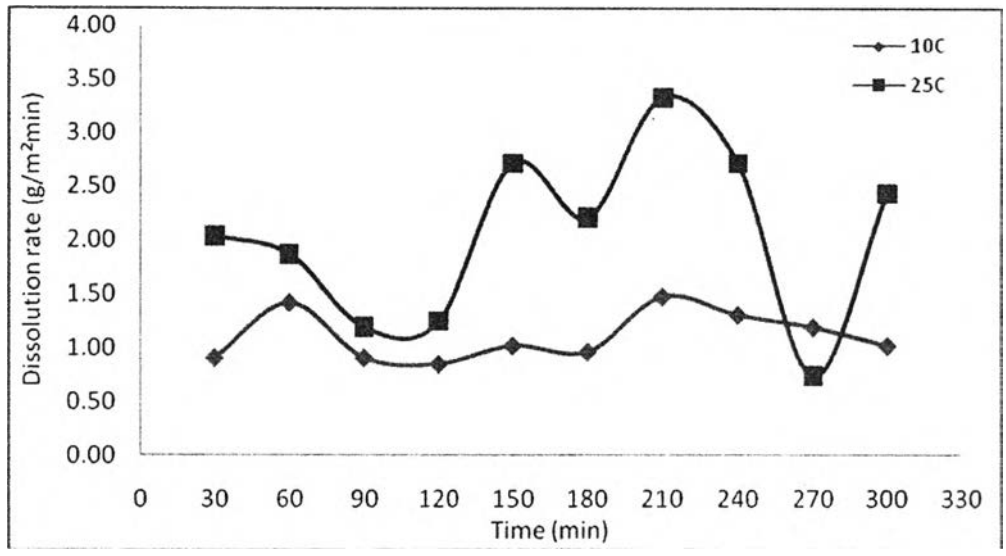

Figure A.15 Dissolution rate with time at different temperatures, 0.21-0.25 mm, 100 defects/cm^3 and 25LPM.

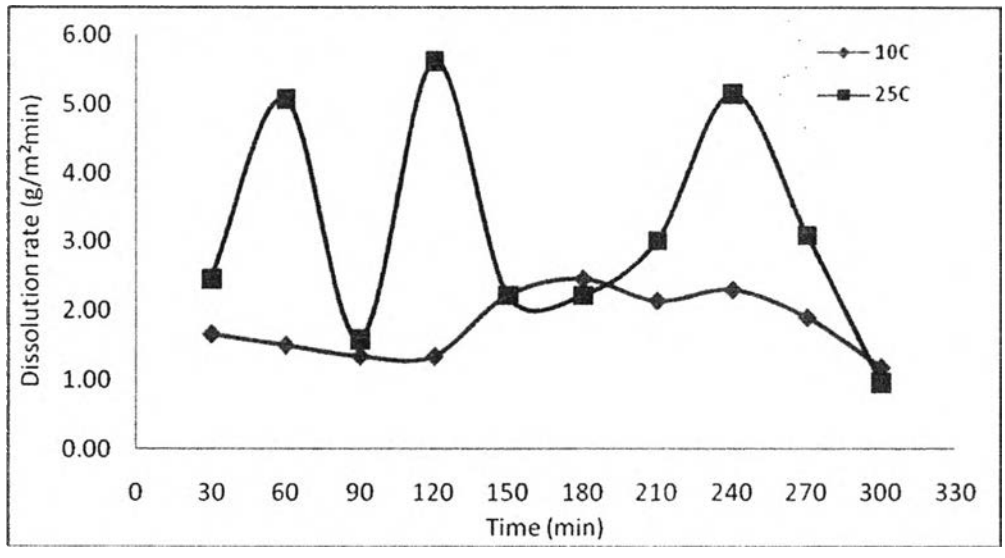

Figure A.16 Dissolution rate with time at different temperatures, 0.21-0.25 mm, 100 defects/cm^3 and 35LPM.

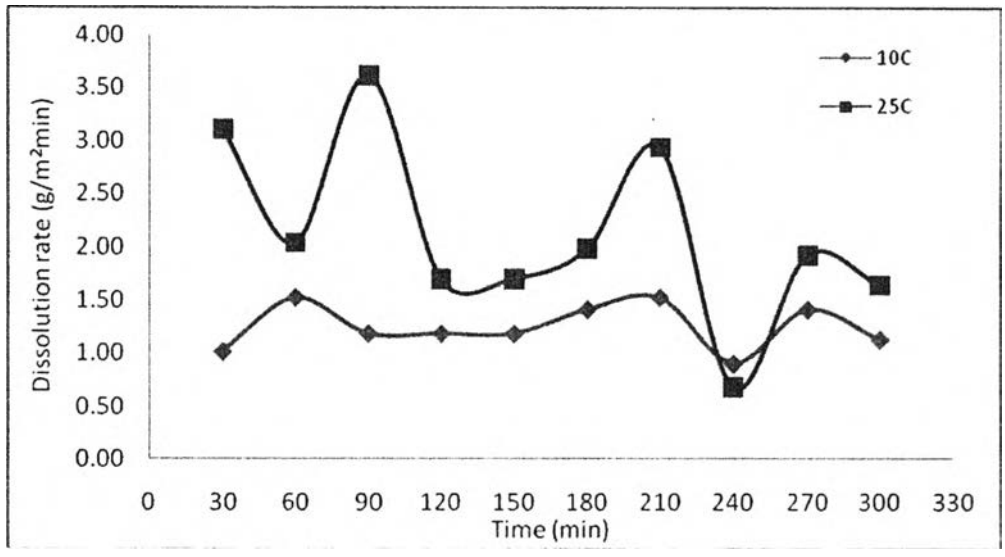

Figure A.17 Dissolution rate with time at different temperatures, 0.42-0.50 mm, 100 defects/cm^3 and 25LPM.

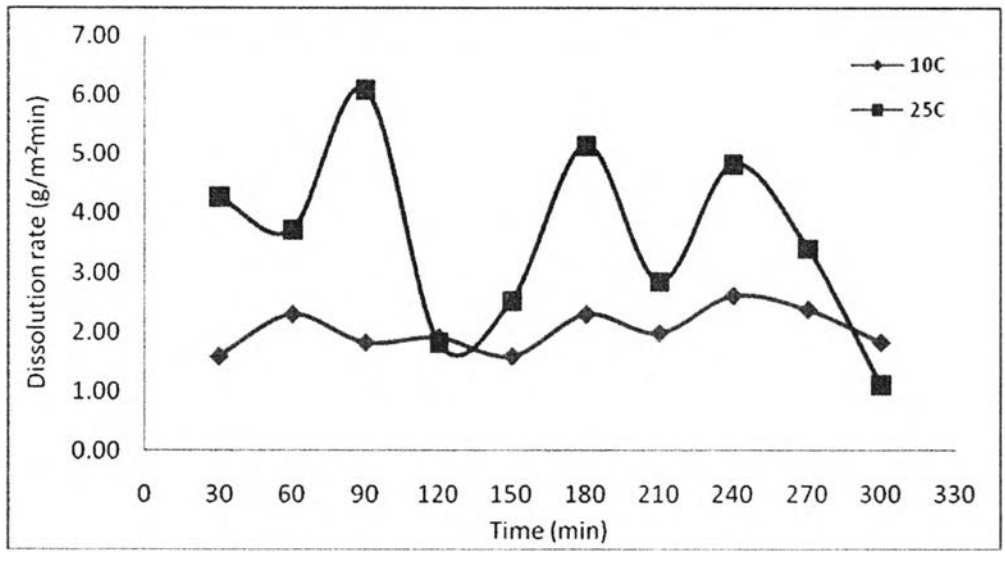

Figure A.18 Dissolution rate with time at different temperatures, 0.42-0.50 mm, 100 defects/cm^3 and 35LPM.

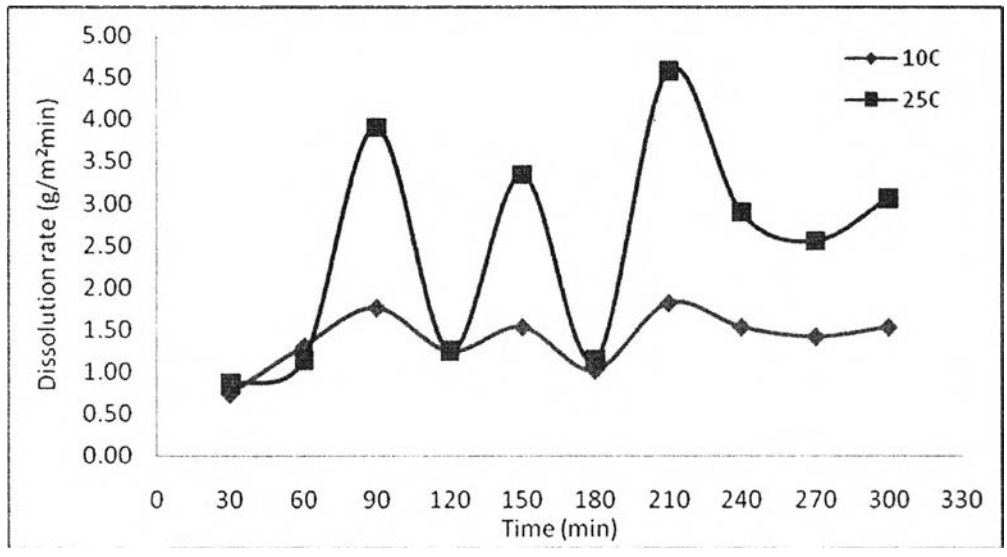

Figure A.19 Dissolution rate with time at different temperatures, 0.500-0.707 mm, 100 defects/cm^3 and 25LPM.

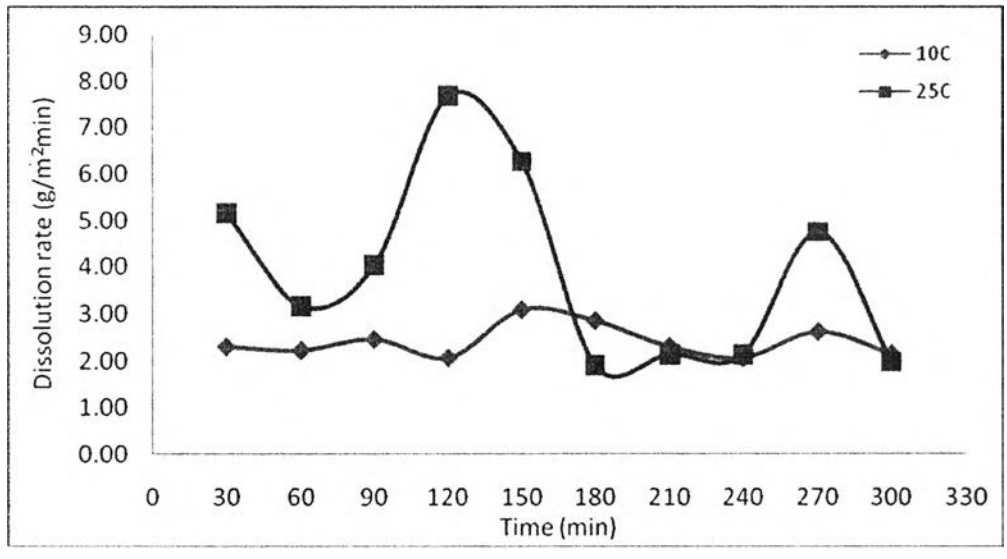

Figure A.20 Dissolution rate with time at different temperatures, 0.500-0.707 mm, 100 defects/cm^3 and 35LPM.

A.2 Dissolution Rate along the Pipe Length

A.2.1 The Effect of Flow Rate

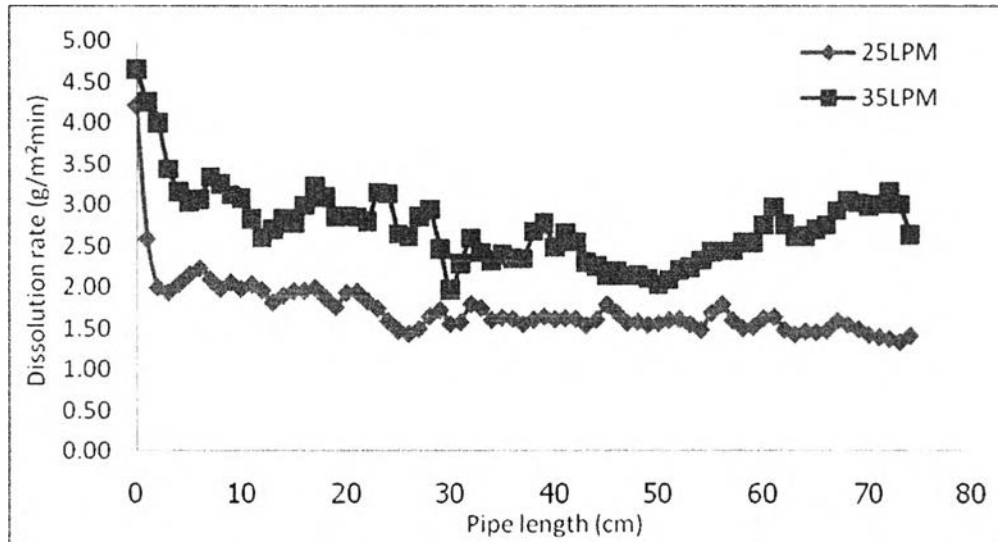

Figure A.21 Dissolution rate along the pipe length under pH7 and 30°C.

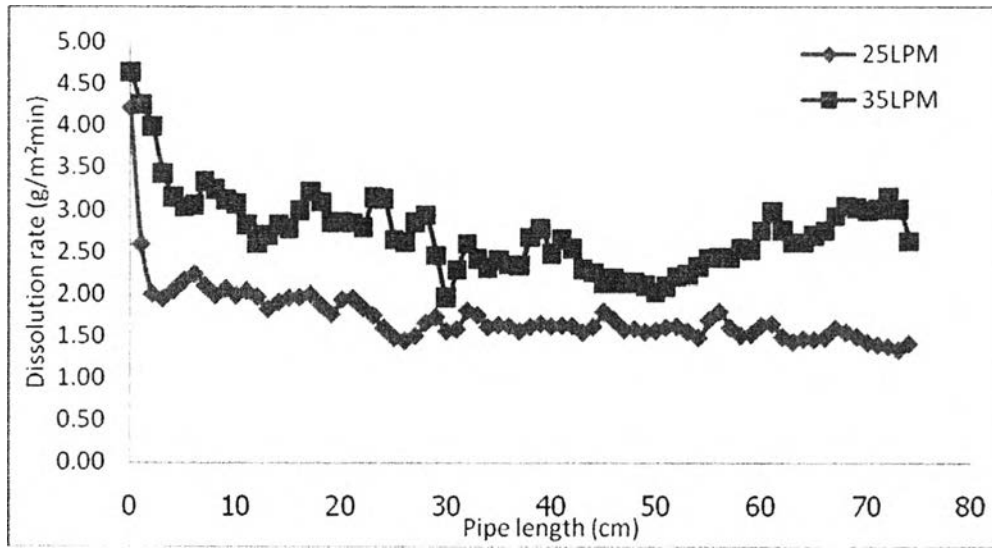

Figure A.22 Dissolution rate along the pipe length under pH10 and 30°C.

A.2.2 Effect of Defect size

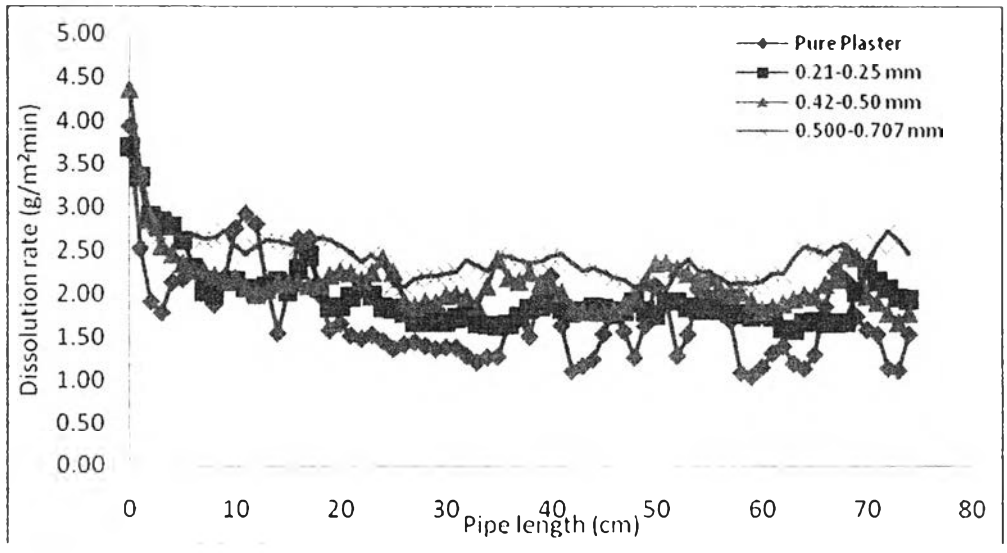

Figure A.23 Dissolution along the pipe at different particle sizes, 100 defects/cm^3, 25LPM and 25°C.

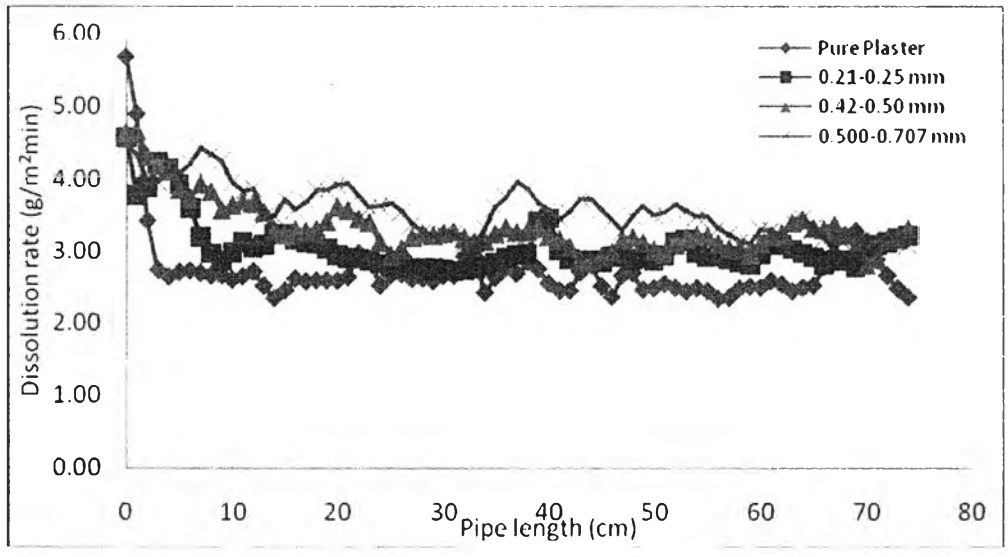

Figure A.24 Dissolution along the pipe at different particle sizes, 100 defects/cm^3,35LPM and 25°C.

Table A.7 Average dissolution rate calculating from the thickness of pipe at different sizes of initial defects and 35 LPM.

Defect Size (mm)	Defect concentration (defects/cm^3)	Flowrate	Average dissolution rate (g/m^{2}min)	Flowrate	Average dissolution rate (g/m^{2}min)
Pure plaster	0	25	1.729	35	2.709
0.21-0.25	100	25	1.967	35	3.054
0.42-0.50	100	25	2.144	35	3.324
0.500-0.707	100	25	2.423	35	3.566

A.2.3 Effect of Defect Concentration

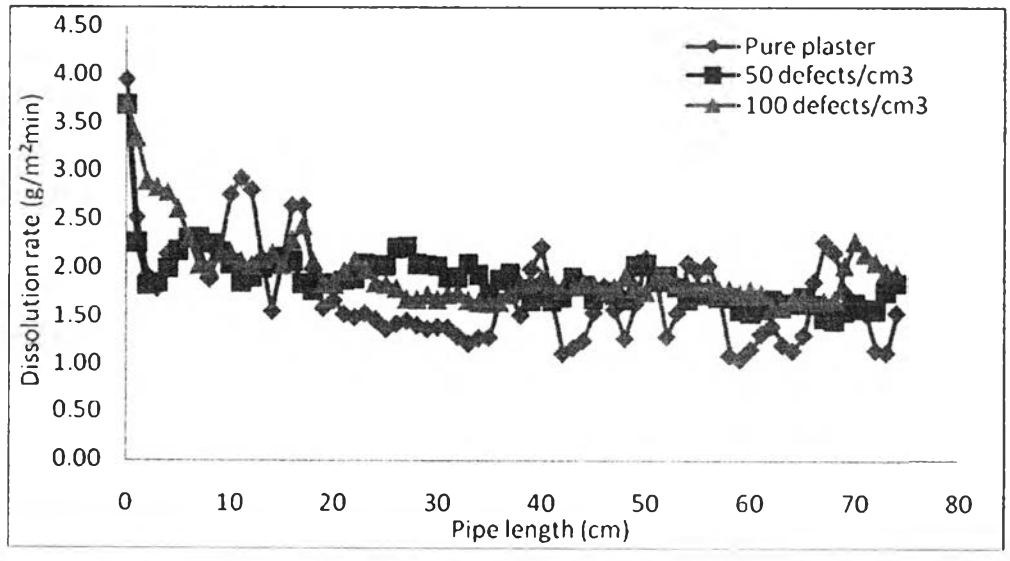

Figure A.25 Dissolution along the pipe at different particle concentrations, 0.21-0.25 mm, 25LPM and 25°C.

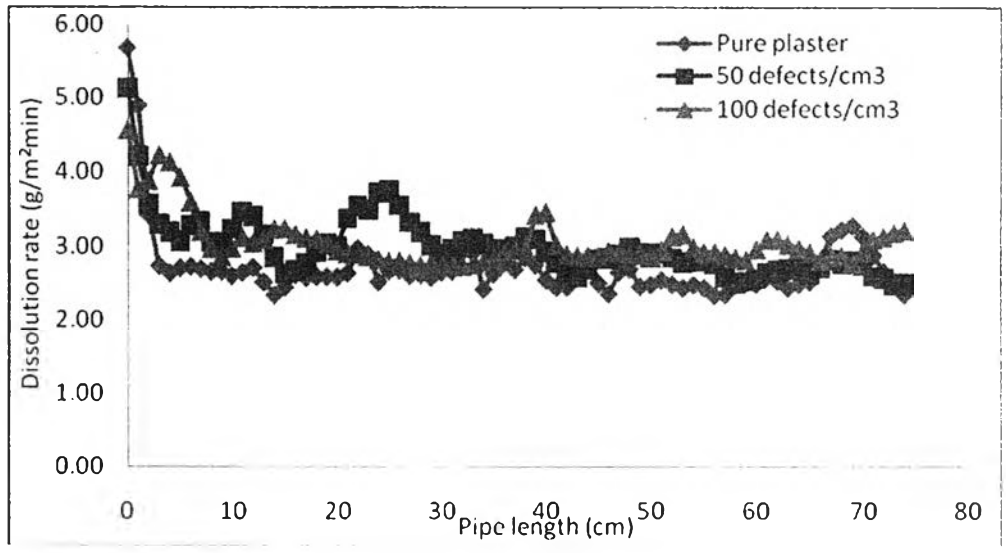

Figure A.26 Dissolution along the pipe at different particle concentrations, 0.21-0.25 mm, 35LPM and 25°C.

Table A.8 Average dissolution rate calculating from the thickness of pipe at different concentrations of initial defects and different flowrates.

Defect Concentration (defects/cm^3)	Defect size (mm)	Flowrate (LPM)	Average dissolution rate (g/m^{2}min)	Flowrate (LPM)	Average dissolution rate (g/m^{2}min)
Pure plaster	0	25	1.73	35	2.71
50	0.21-0.25	25	1.87	35	2.99
100	0.21-0.25	25	1.97	35	3.05

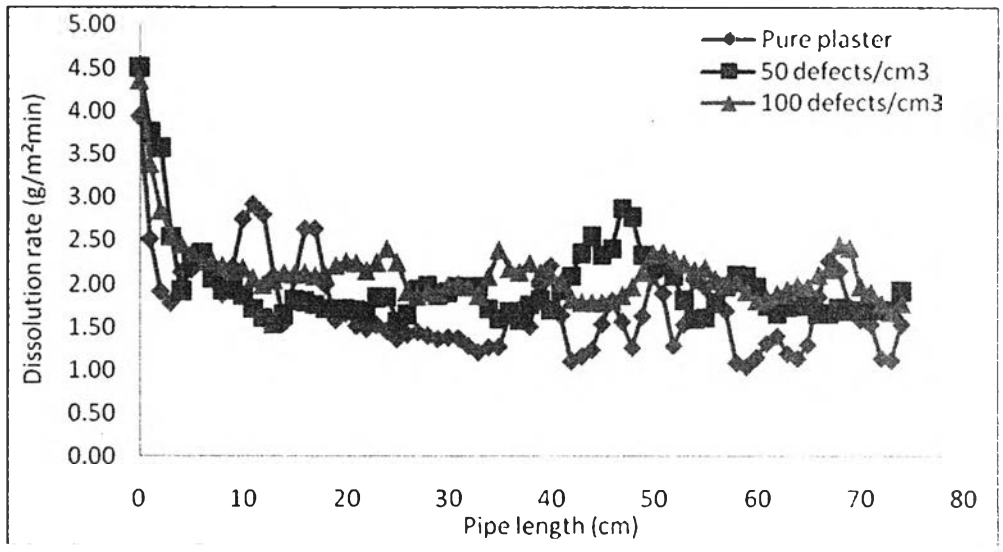

Figure A.27 Dissolution along the pipe at different particle concentrations, 0.42-0.50 mm, 25LPM and 25°C.

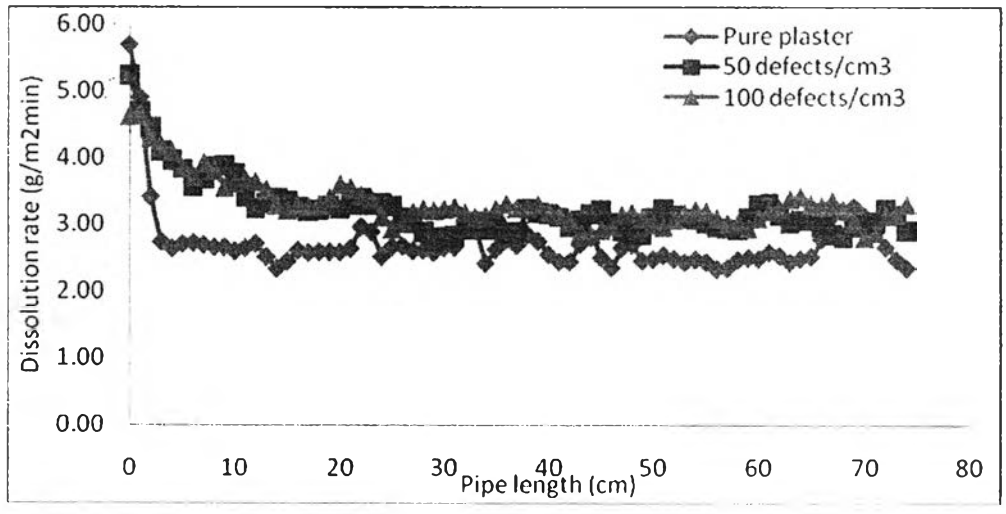

Figure A.28 Dissolution along the pipe at different particle concentrations, 0.42-0.50 m, 35LPM and 25°C.

Table A.9 Average dissolution rate calculating from the thickness of pipe at different concentrations of initial defects and different flowrate.

Defect Concentration (defects/cm^3)	Defect size (mm)	Flowrate (LPM)	Average dissolution rate (g/m^{2}min)	Flowrate (LPM)	Average dissolution rate (g/m^{2}min)
Pure plaster	0	25	1.73	35	2.71
50	0.42-0.50	25	1.99	35	3.24
100	0.42-0.50	25	2.14	35	3.32

A.2.4 Effect of Temperature

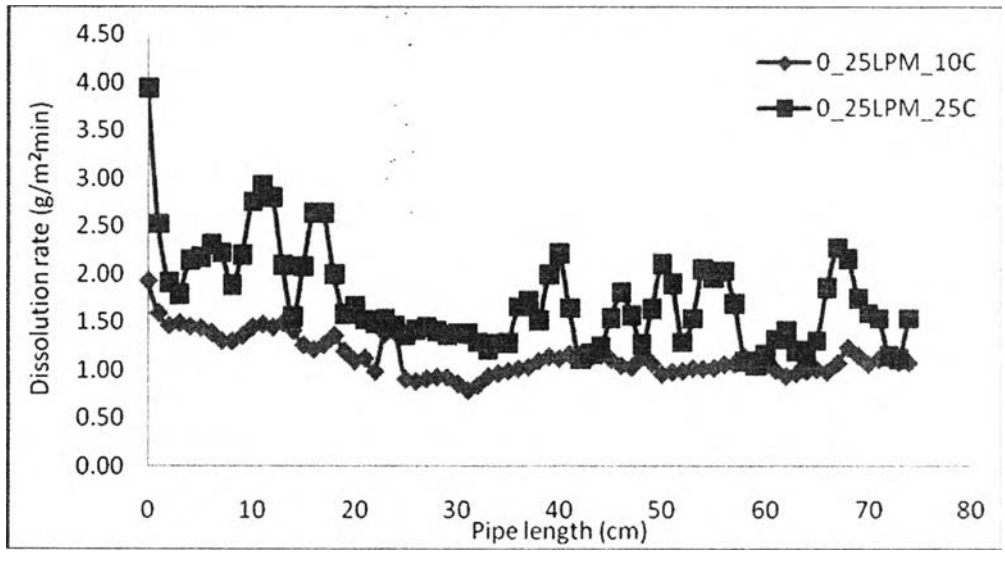

Figure A.29 Dissolution along the pipe at different temperatures, pure plaster, and 25LPM.

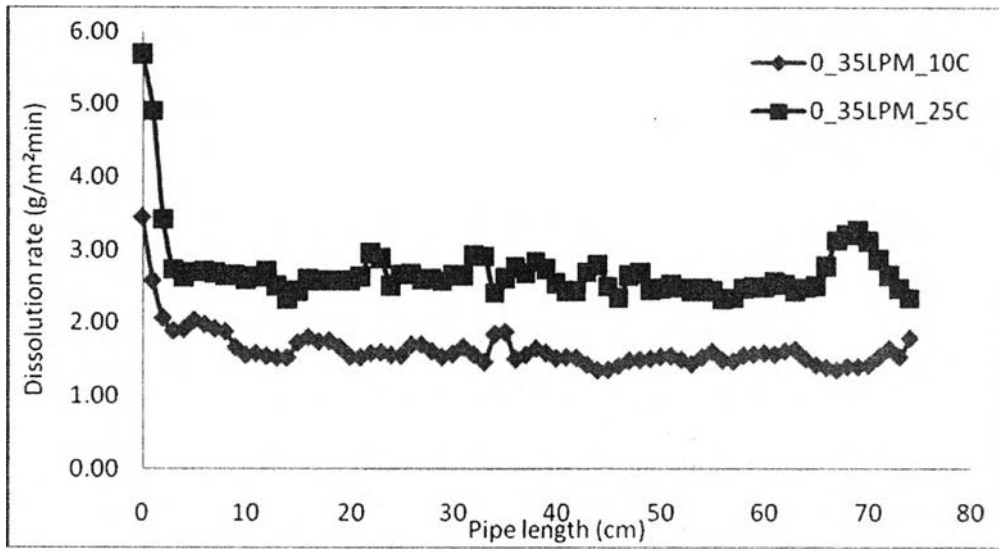

Figure A.30 Dissolution along the pipe at different temperatures, pure plaster, and 35LPM.

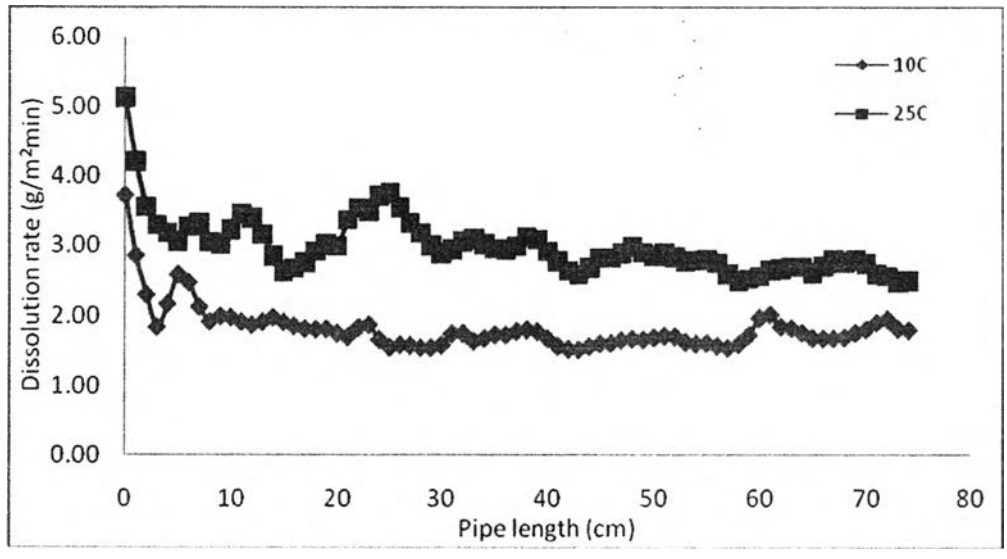

Figure A.31 Dissolution along the pipe at different temperatures, 0.21-0.25, 50 defects/cm^3 and 35LPM.

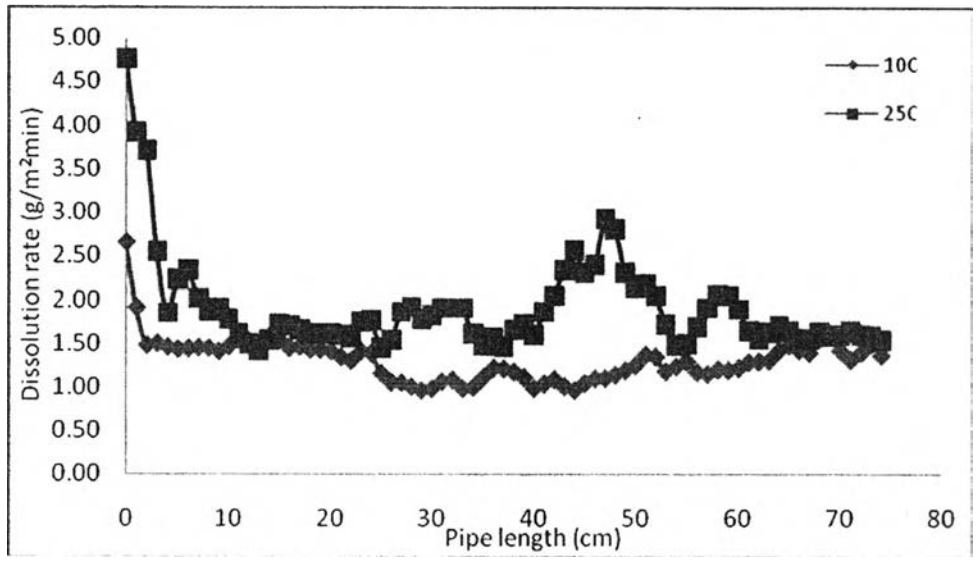

Figure A.32 Dissolution along the pipe at different temperatures, 0.42-0.50, 50 defects/cm^3 and 25LPM.

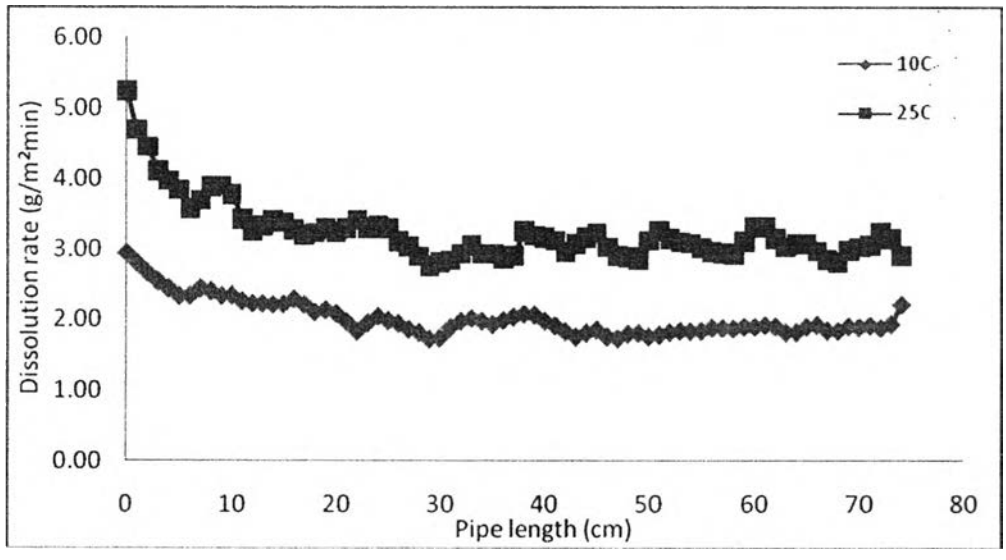

Figure A.33 Dissolution along the pipe at different temperatures, 0.42-0.50, 50 defects/cm^3 and 35LPM.

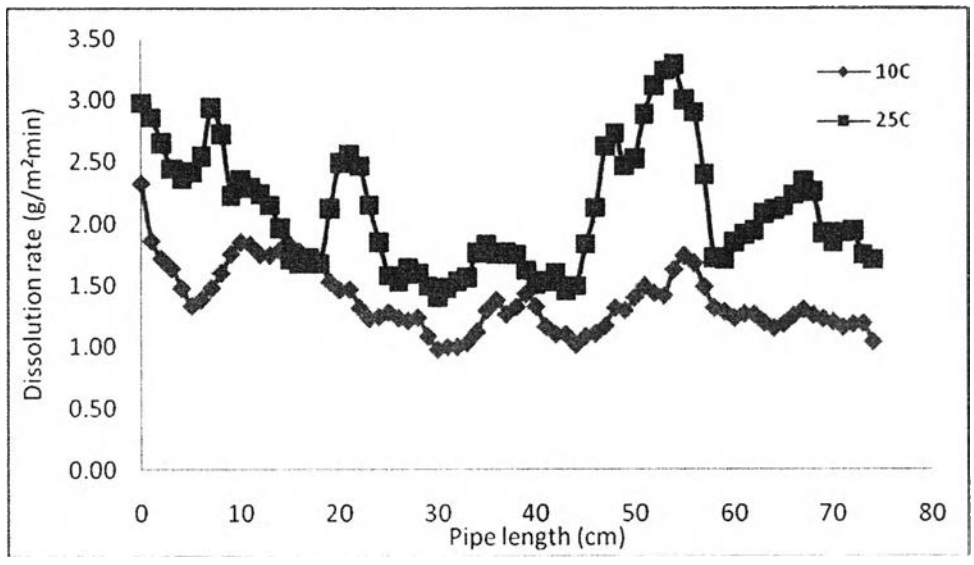

Figure A.34 Dissolution along the pipe at different temperatures, 0.500-0.707, 50 defects/cm^3 and 25LPM.

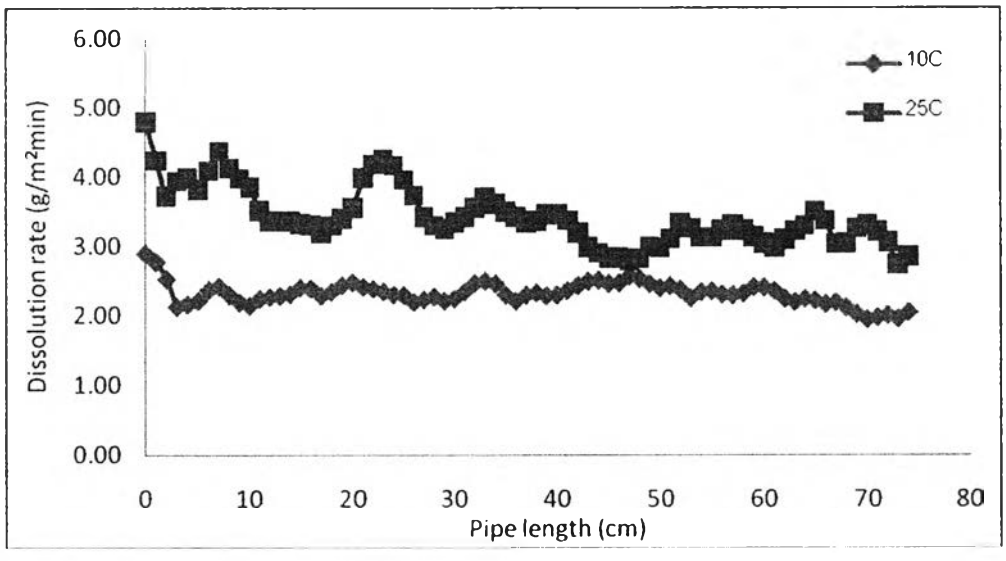

Figure A.35 Dissolution along the pipe at different temperatures, 0.500-0.707, 50 defects/cm^3 and 35LPM.

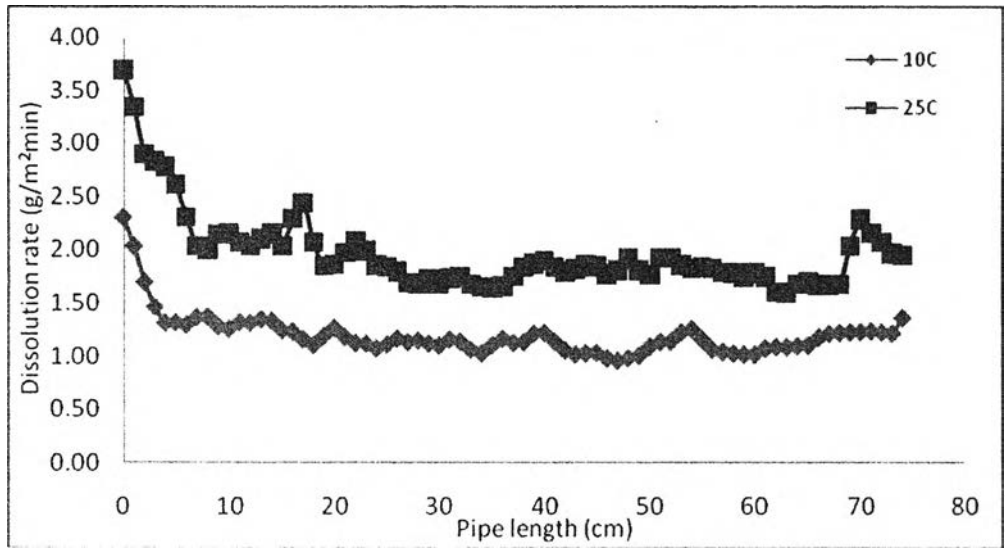

Figure A.36 Dissolution along the pipe at different temperatures, 0.21-0.25, 100 defects/cm^3 and 25LPM.

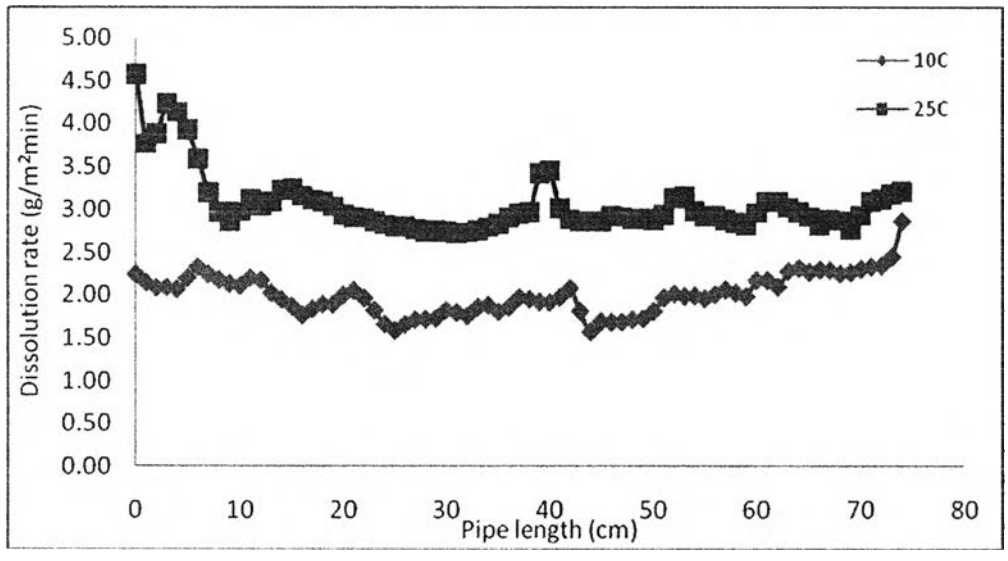

Figure A.37 Dissolution along the pipe at different temperatures, 0.21-0.25, 100 defects/cm^3 and 35LPM.

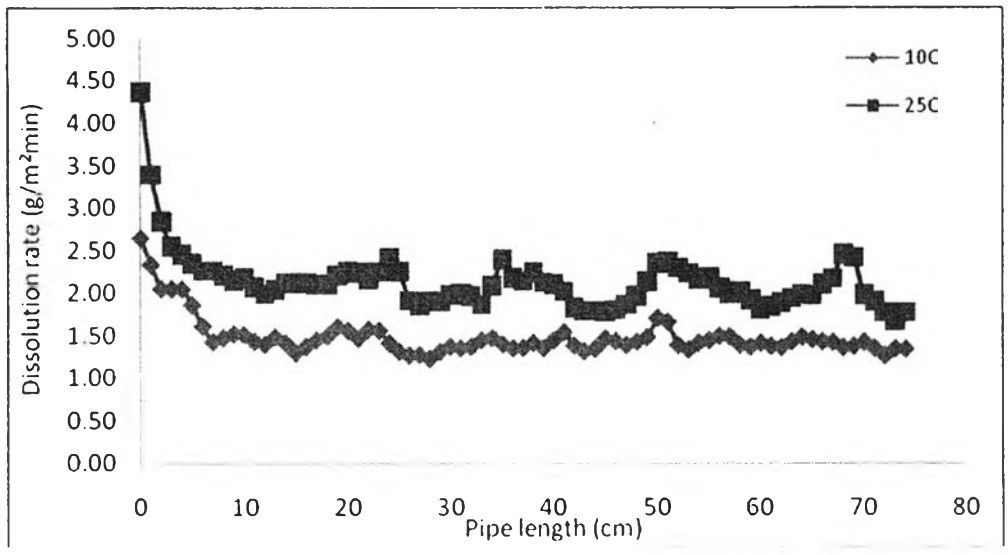

Figure A.38 Dissolution along the pipe at different temperatures, 0.42-0.50, 100 defects/cm^3 and 25LPM.

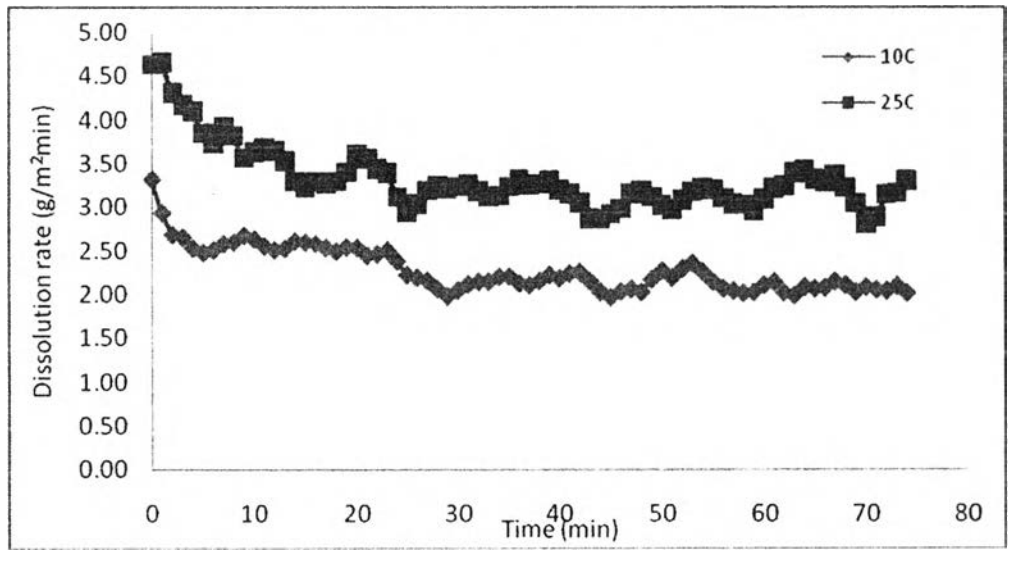

Figure A.39 Dissolution along the pipe at different temperatures, 0.42-0.50, 100 defects/cm^3 and 35LPM.

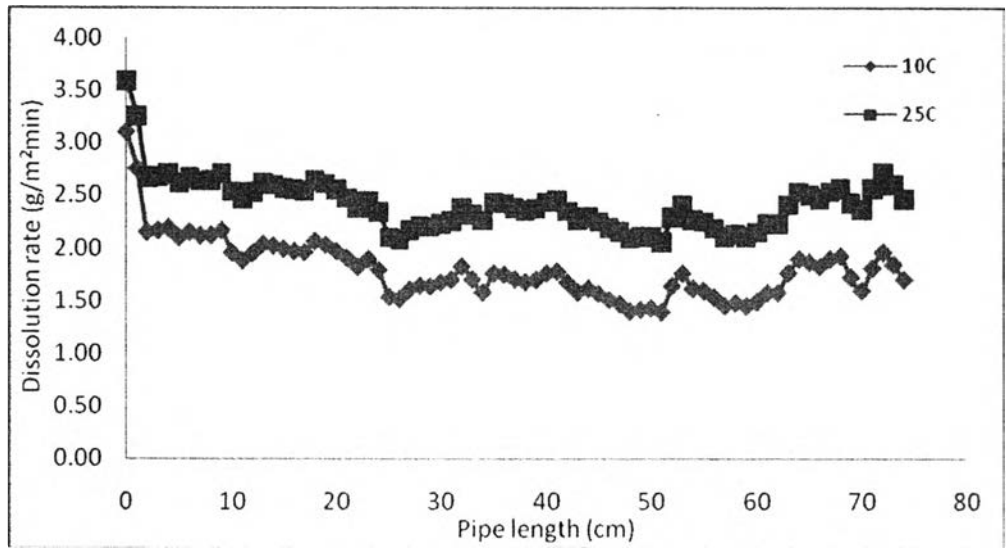

Figure A.40 Dissolution along the pipe at different temperatures, 0.500-0.707, 100 defects/cm^3 and 25LPM.

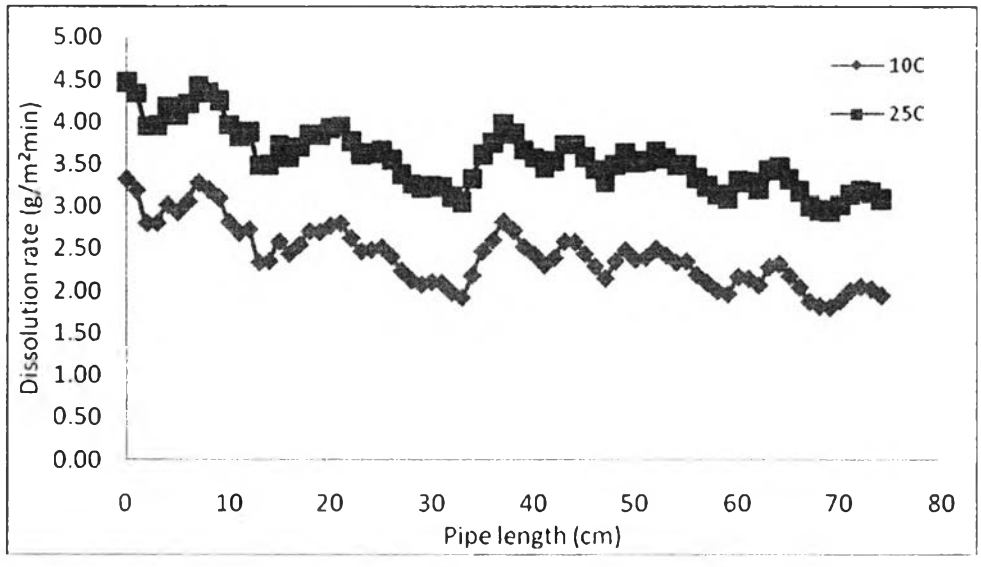

Figure A.41 Dissolution along the pipe at different temperatures, 0.500-0.707, 100 defects/cm^3 and 35LPM.

Appendix B Pressure Drop

B.1 The Effect of Flow Rate

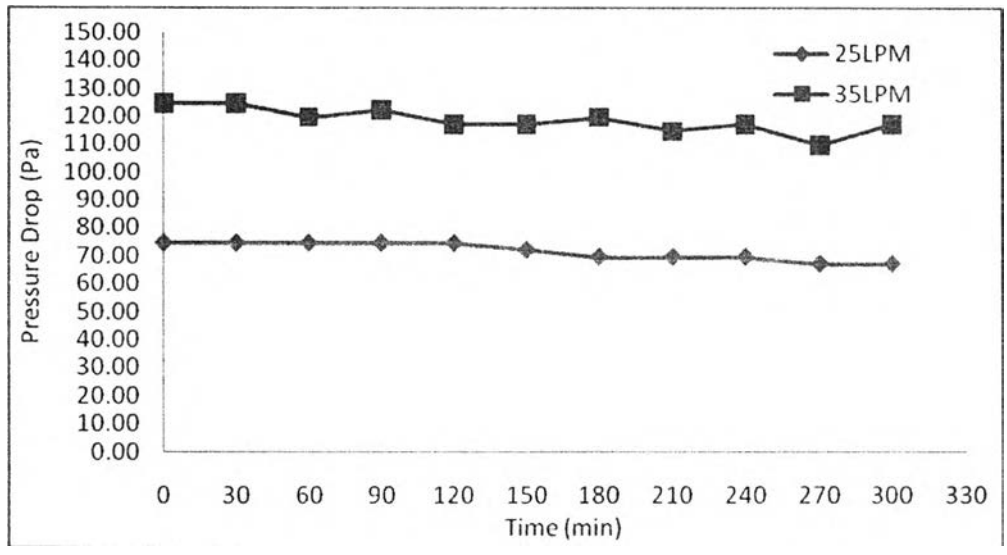

Table B.1 Pressure drop under pH7 and 30°C.

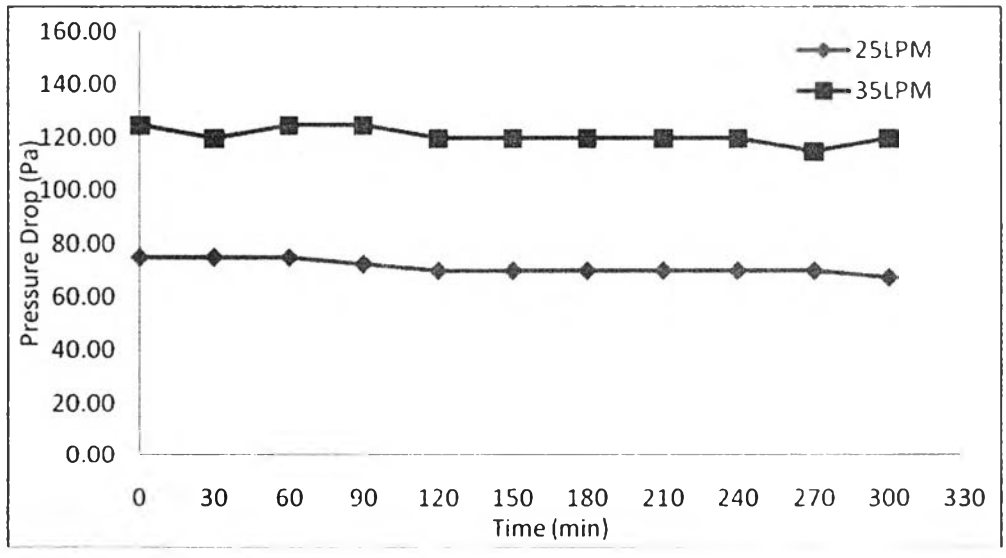

Figure B.2 Pressure drop under pH10 and 30°C.

B.2 Effect of Defect Size

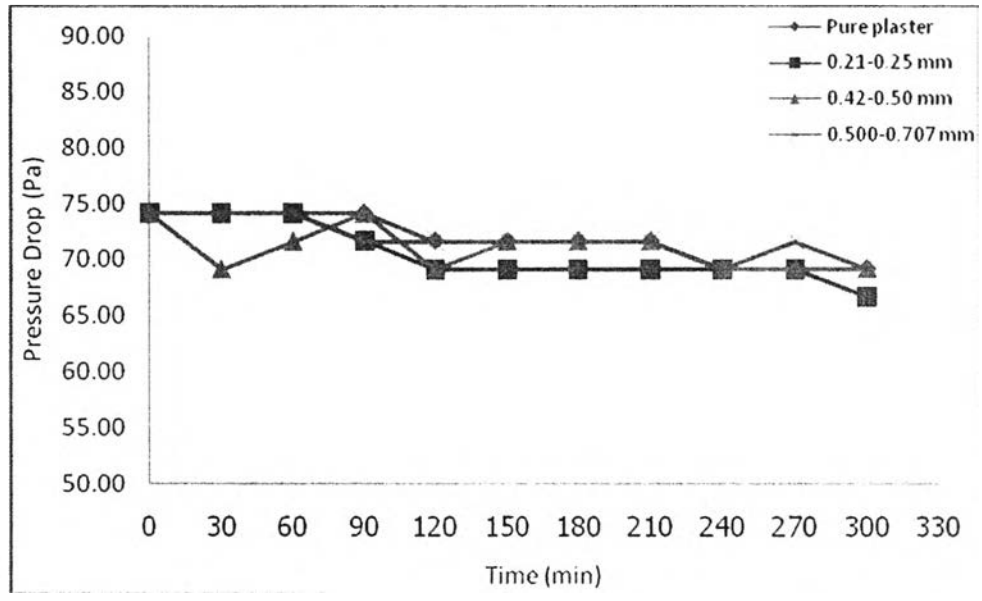

Figure B.3 Pressure drop at different size of particles, 100 defects/cm^3, 25°C and 25 LPM.

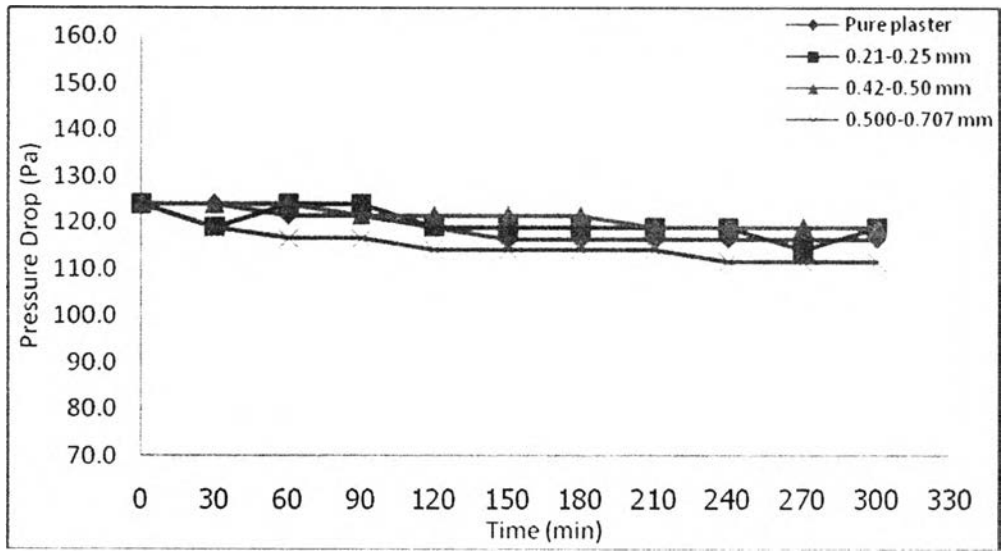

Figure B.4 Pressure drop at different size of particles, 100 defects/cm^3, 25°C and 35 LPM.

B.3 Effect of Defect Concentration

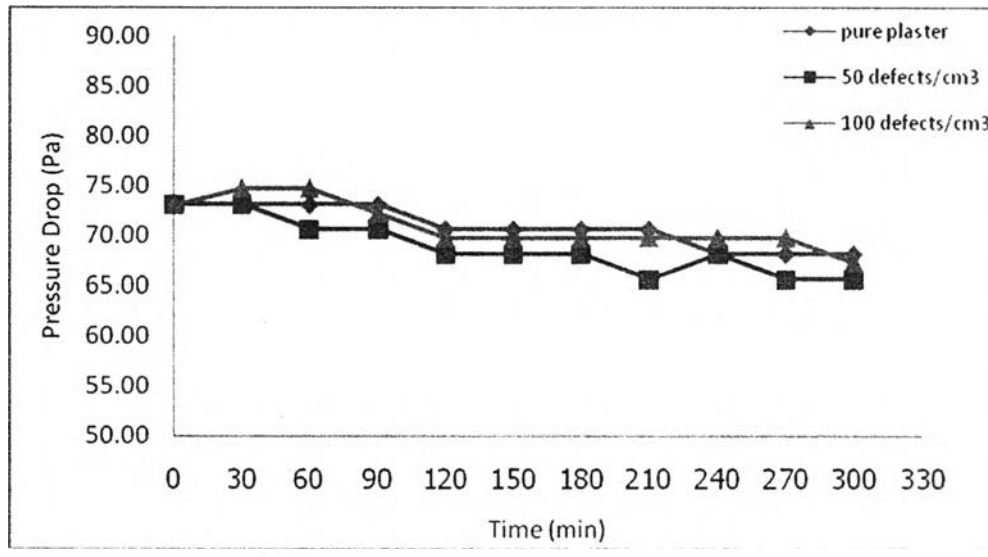

Figure B.5 Pressure drop with time at different concentrations of particles, 0.21-0.25 mm, 25°C and 25 LPM.

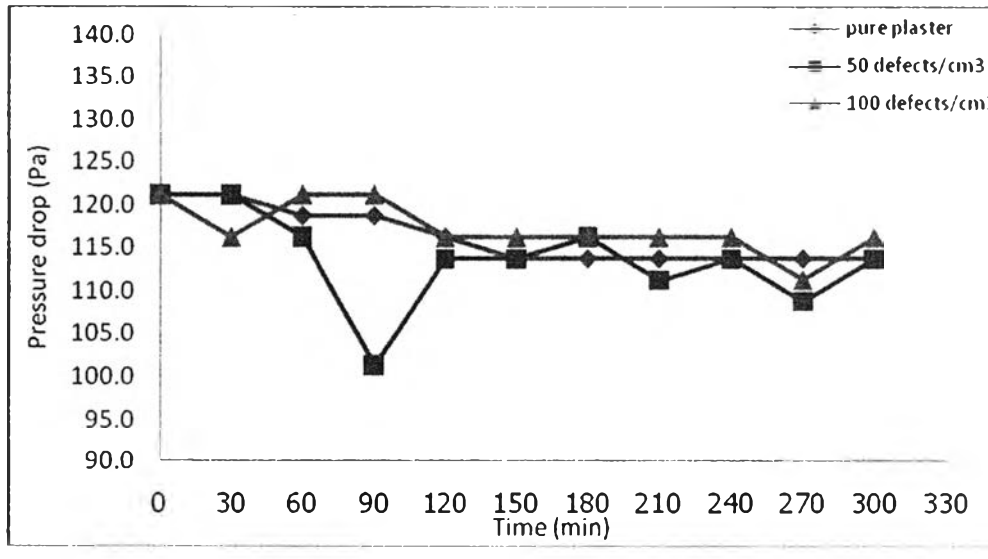

Figure B.6 Pressure drop with time at different concentrations of particles, 0.21-0.25 mm, 25°C and 35 LPM.

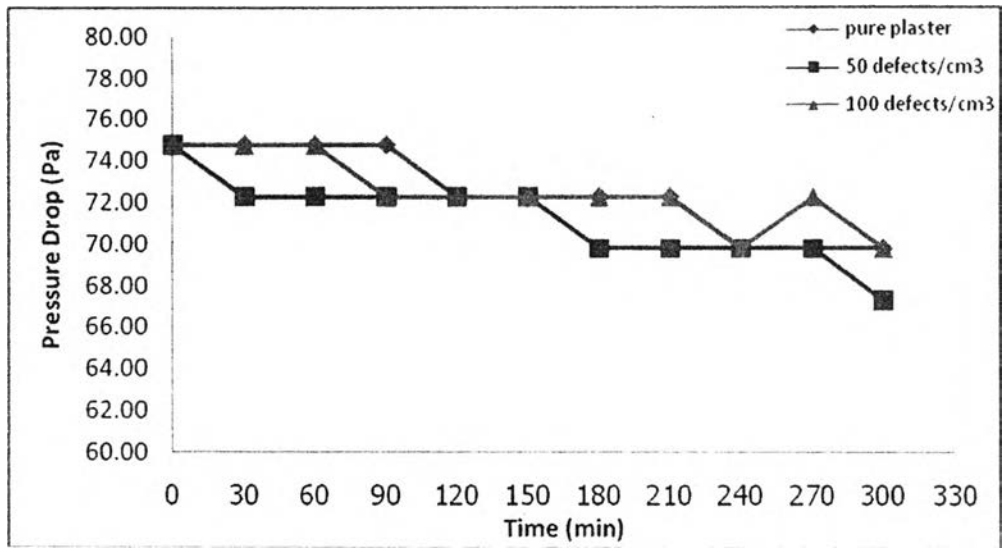

Figure B.7 Pressure drop with time at different concentrations of particles, 0.500-0.707 mm, 25°C and 25 LPM.

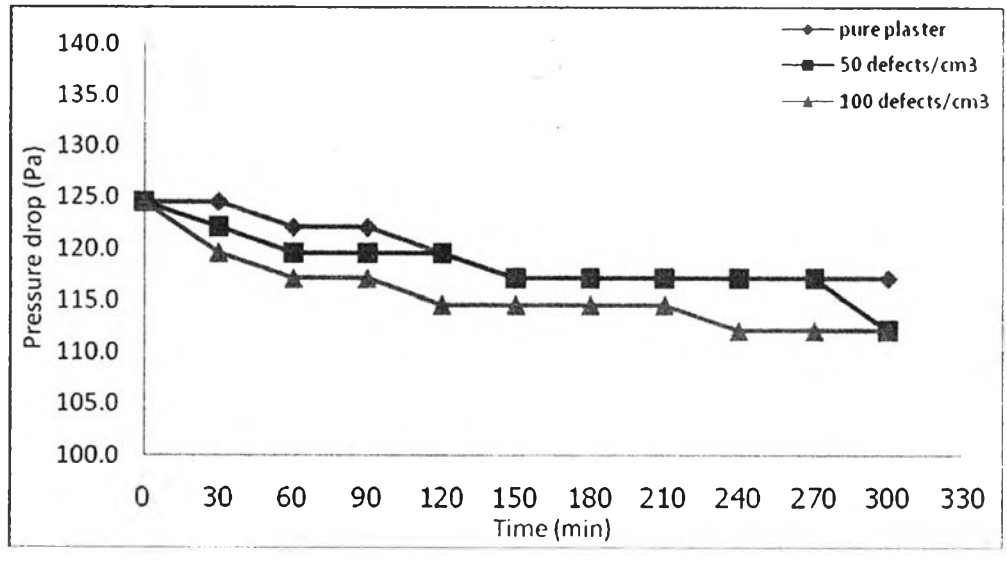

Figure B.8 Pressure drop with time at different concentrations of particles, 0.500-0.707 mm, 25°C and 35 LPM.

B.4 Effect of Temperature

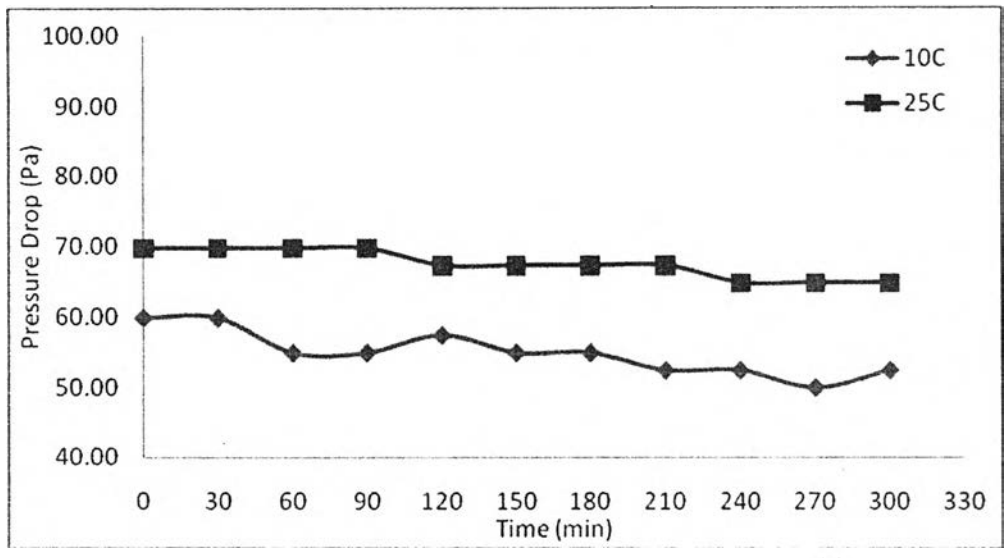

Figure B.9 Pressure drop with time at different temperatures, pure plaster and 25 LPM.

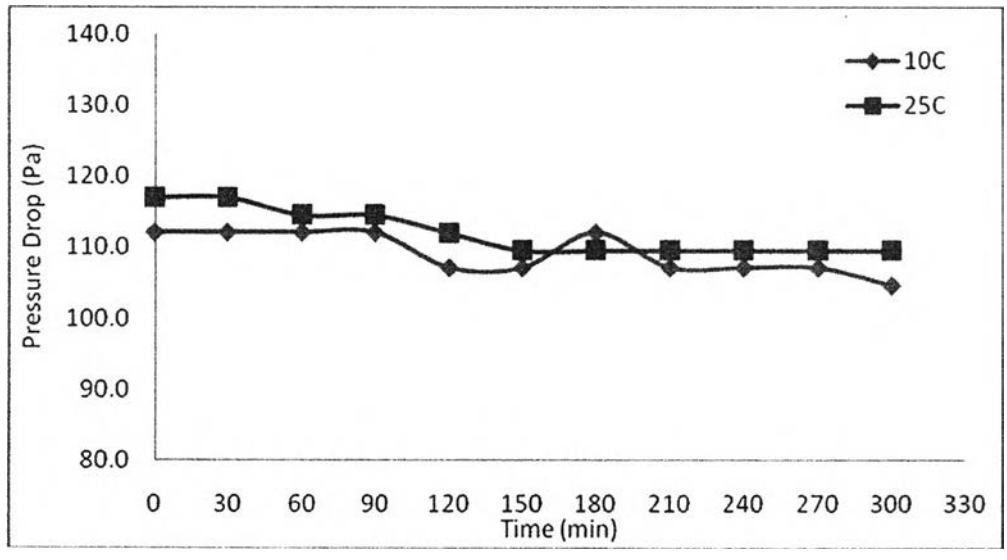

Figure B.10 Pressure drop with time at different temperatures, pure plaster and 35 LPM.

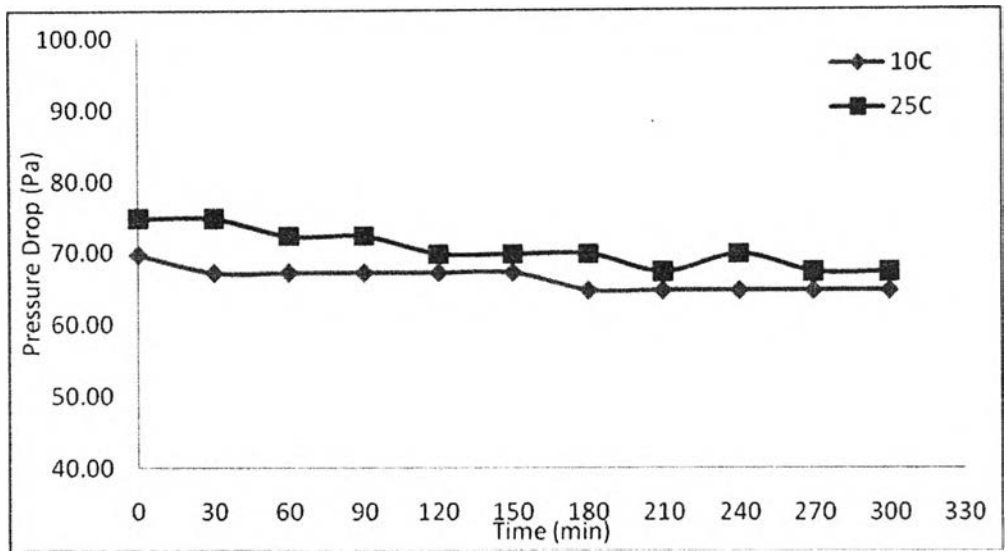

Figure B.11 Pressure drop with time at different temperatures, 0.42-0.50, 50 defects/cm^3 and 25 LPM.

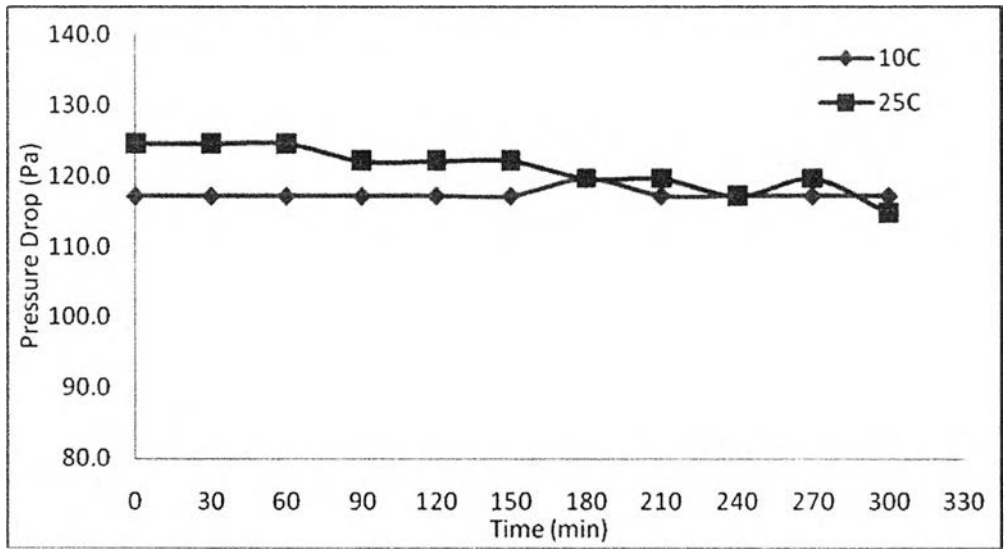

Figure B.12 Pressure drop with time at different temperatures, 0.42-0.50, 50 defects/cm^3 and 35 LPM.

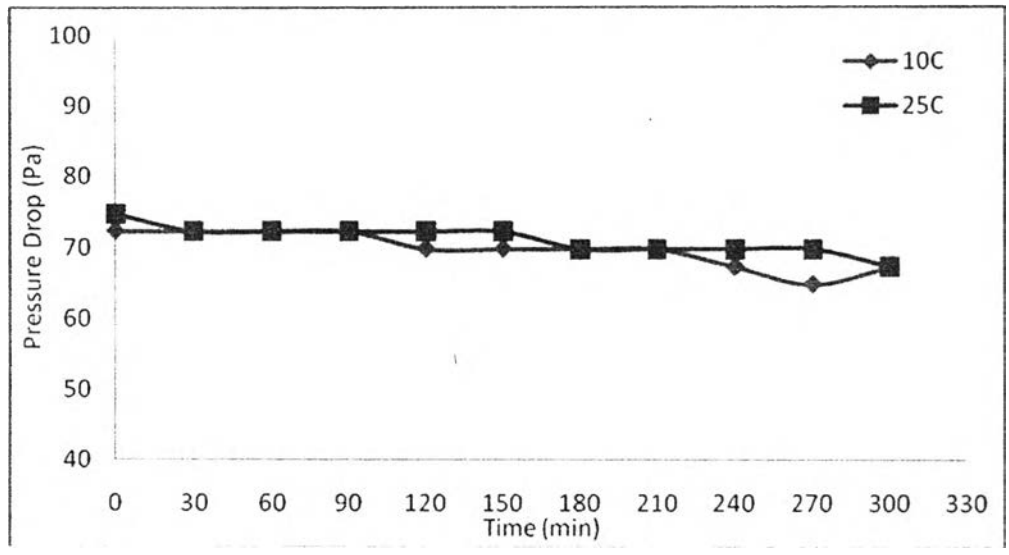

Figure B.13 Pressure drop with time at different temperatures, 0.500-0.707, 50 defects/cm^3 and 25 LPM.

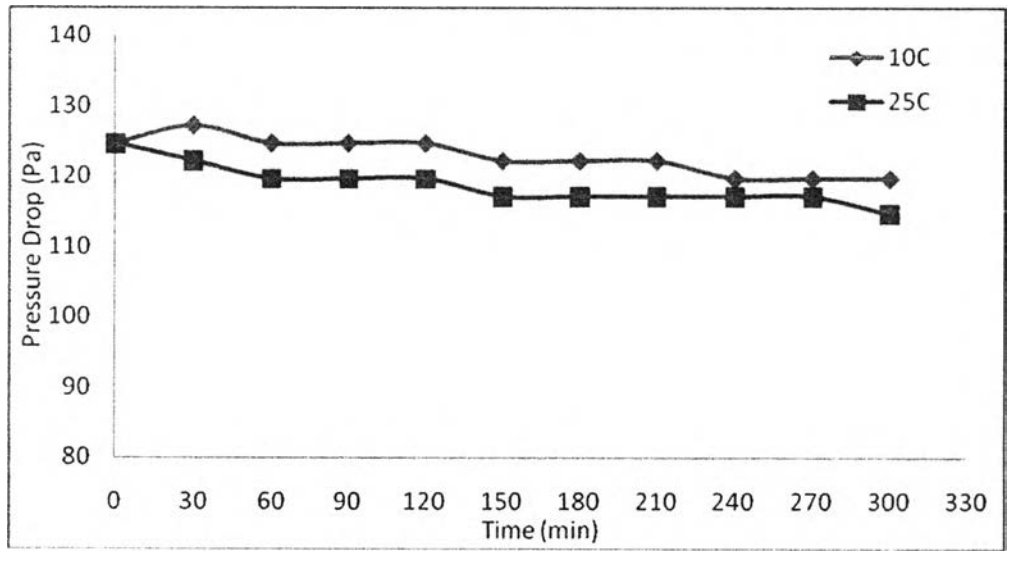

Figure B.14 Pressure drop with time at different temperatures, 0.500-0.707, 50 defects/cm^3 and 35 LPM.

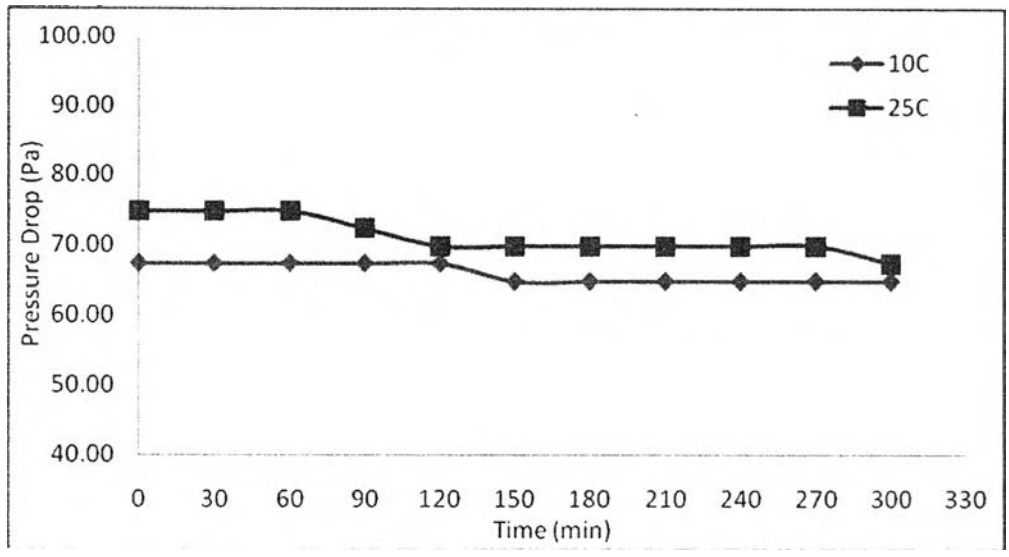

Figure B.15 Pressure drop with time at different temperatures, 0.21-0.25, 100 defects/cm^3 and 25 LPM.

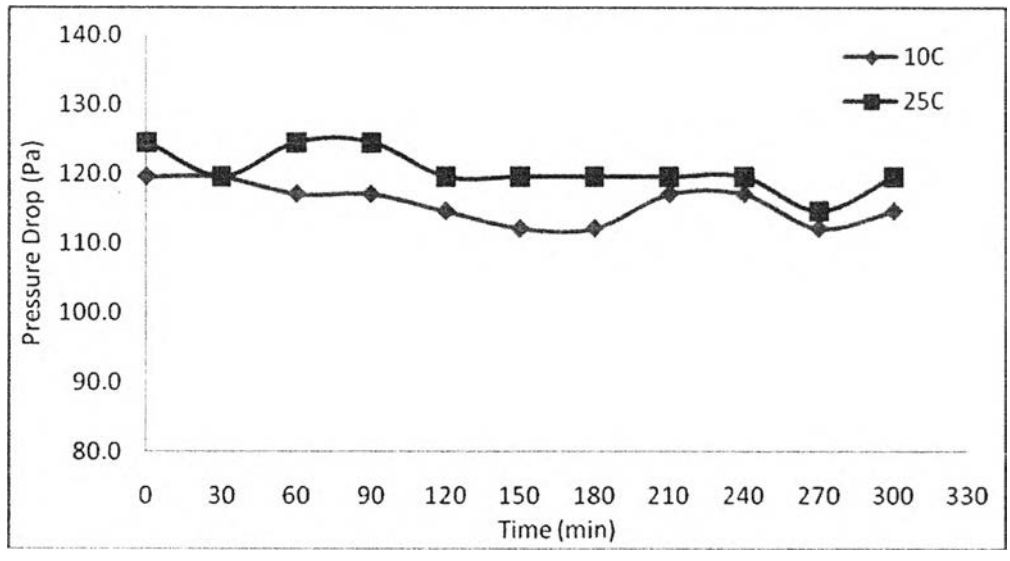

Figure B.16 Pressure drop with time at different temperatures, 0.21-0.25, 100 defects/cm^3 and 35 LPM.

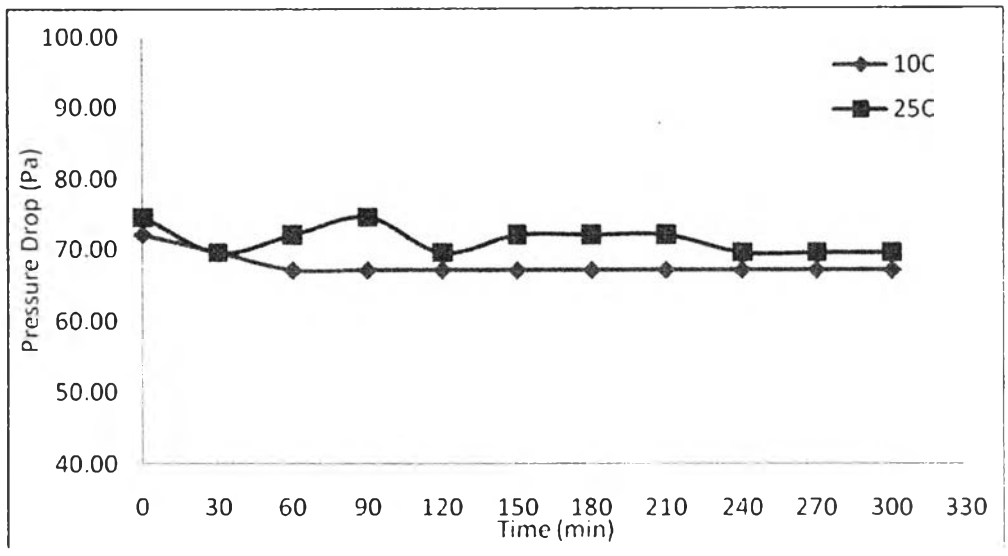

Figure B.17 Pressure drop with time at different temperatures, 0.42-0.50, 100 defects/cm^3 and 25 LPM.

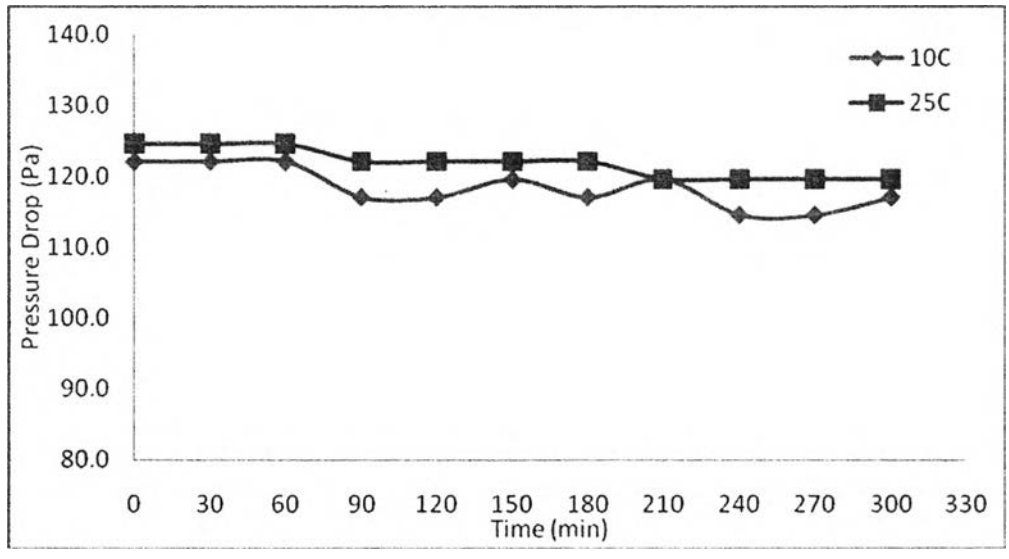

Figure B.18 Pressure drop with time at different temperatures, 0.42-0.50, 100 defects/cm^3 and 35 LPM.

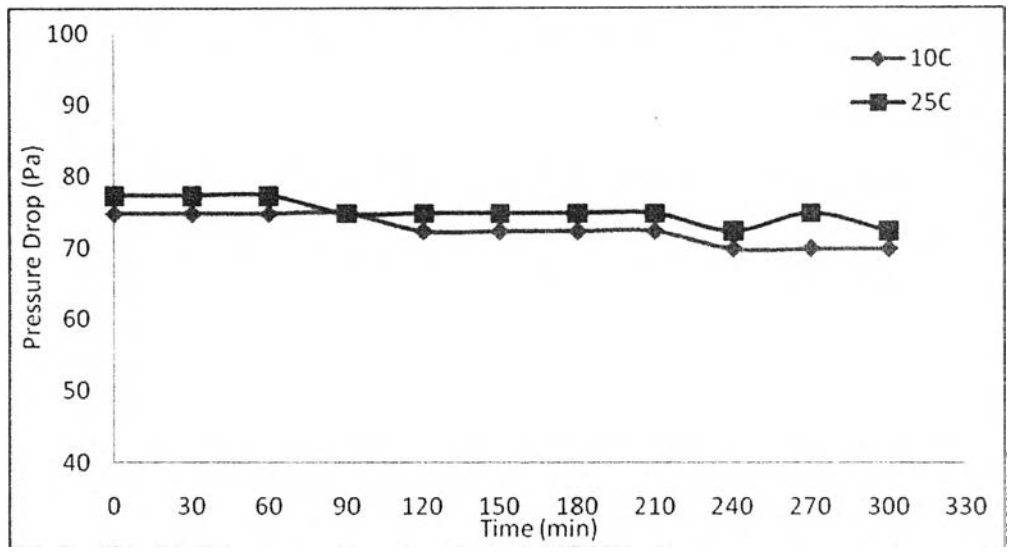

Figure B.19 Pressure drop with time at different temperatures, 0.500-0.707, 100 defects/cm^3 and 25 LPM.

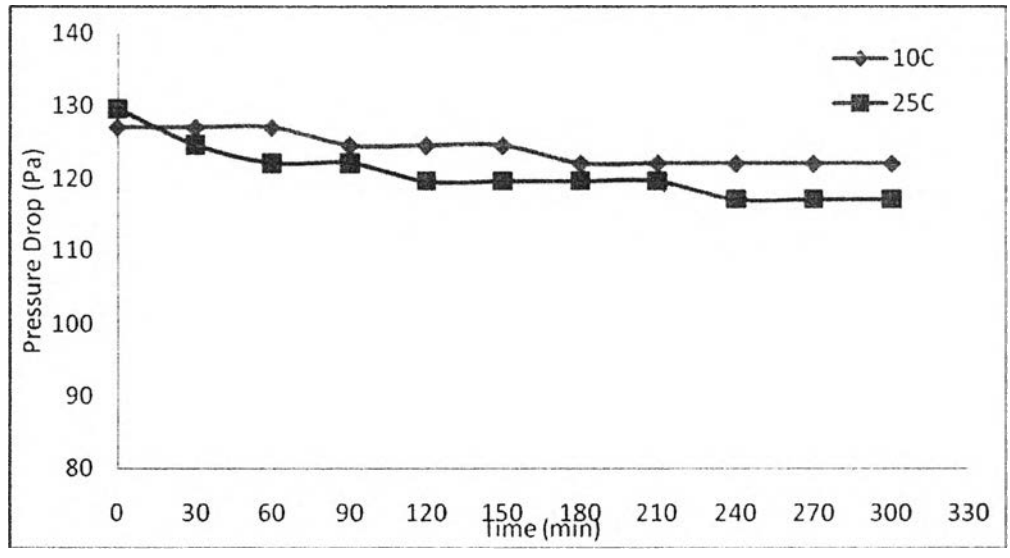

Figure B.20 Pressure drop with time at different temperatures, 0.500-0.707, 100 defects/cm^3 and 35 LPM.

Appendix C The Mechanism of Gypsum Dissolution

C.1 Effect of Flow rate

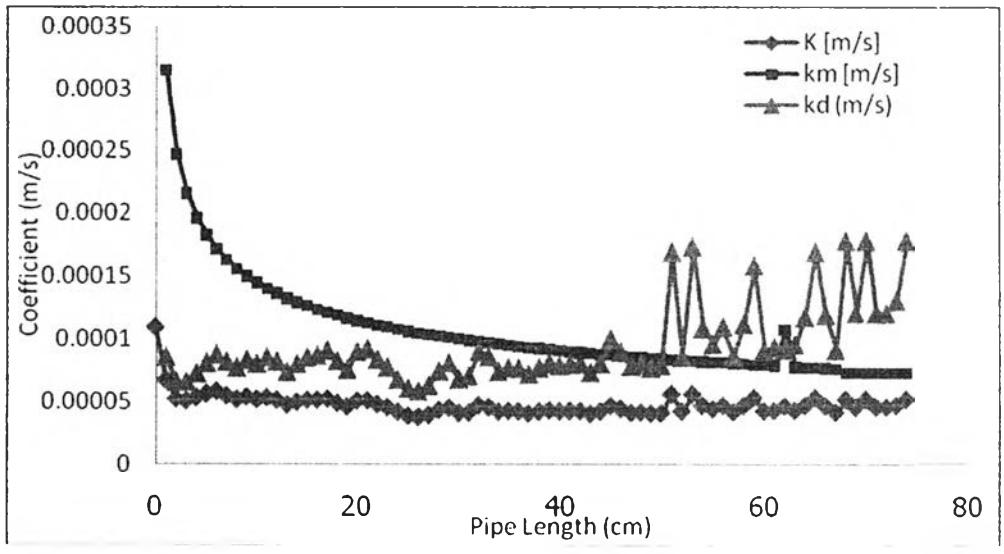

Figure C.1 The overall rate constant (K) and the dissolution coefficient (k_d) compared with the mass transfer coefficient (k_m) along the pipe length under condition pH7, 30°C and 25 LPM.

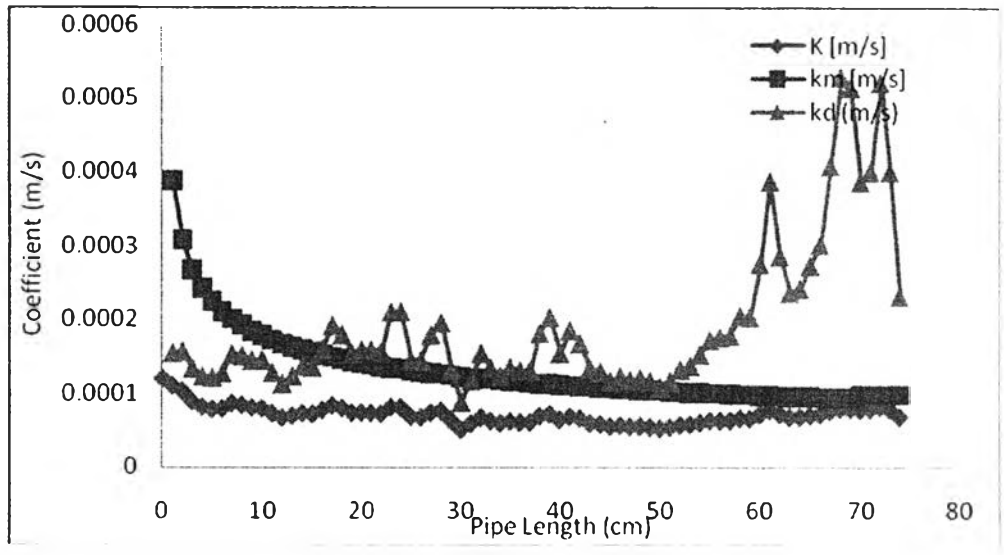

Figure C.2 The overall rate constant (K) and the dissolution coefficient (k_d) compared with the mass transfer coefficient (k_m) along the pipe length under condition pH7, 30°C and 35 LPM.

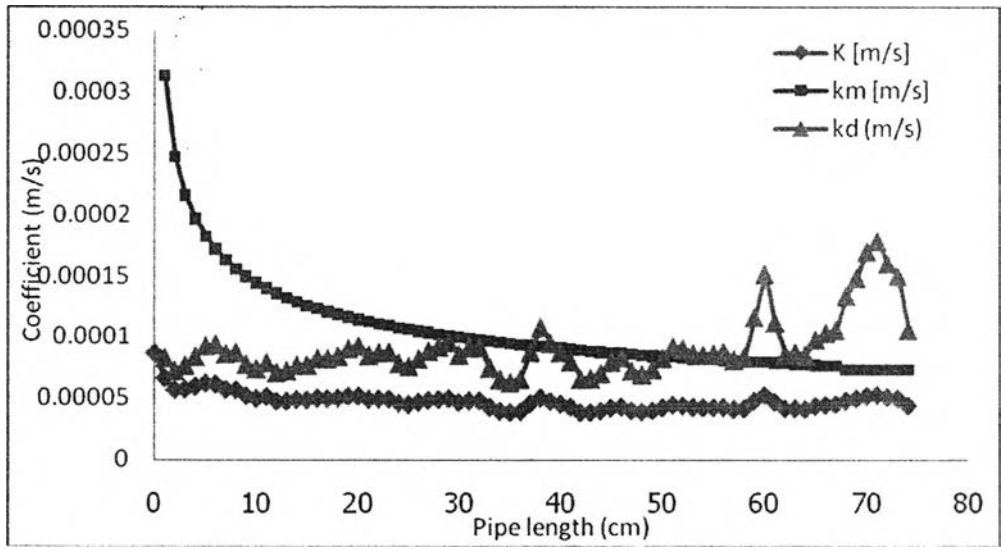

Figure C.3 The overall rate constant (K) and the dissolution coefficient (k_d) compared with the mass transfer coefficient (k_m) along the pipe length under condition pH10, 30°C and 25 LPM.

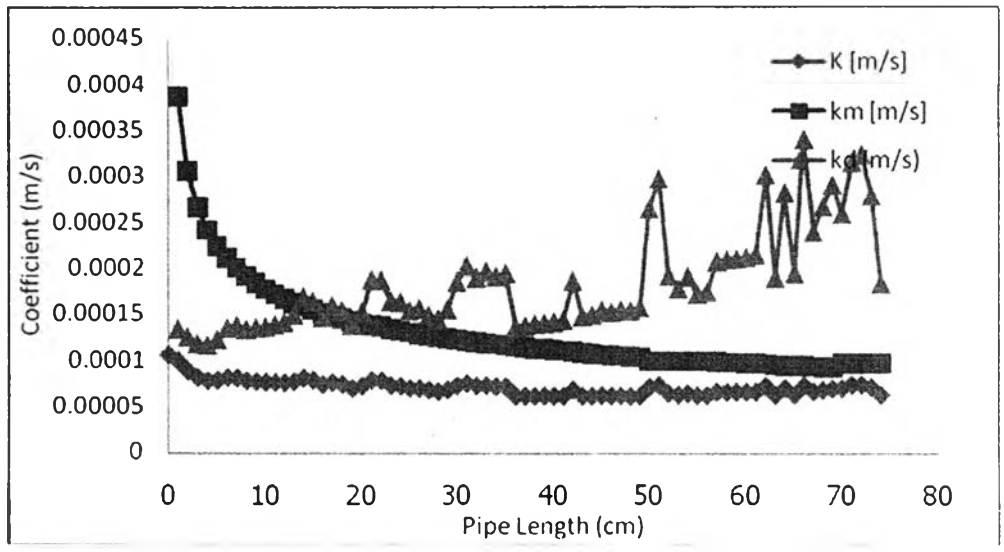

Figure C.4 The overall rate constant (K) and the dissolution coefficient (k_d) compared with the mass transfer coefficient (k_m) along the pipe length under condition pH10, 30°C and 35 LPM.

C.2 Effect of Defect size

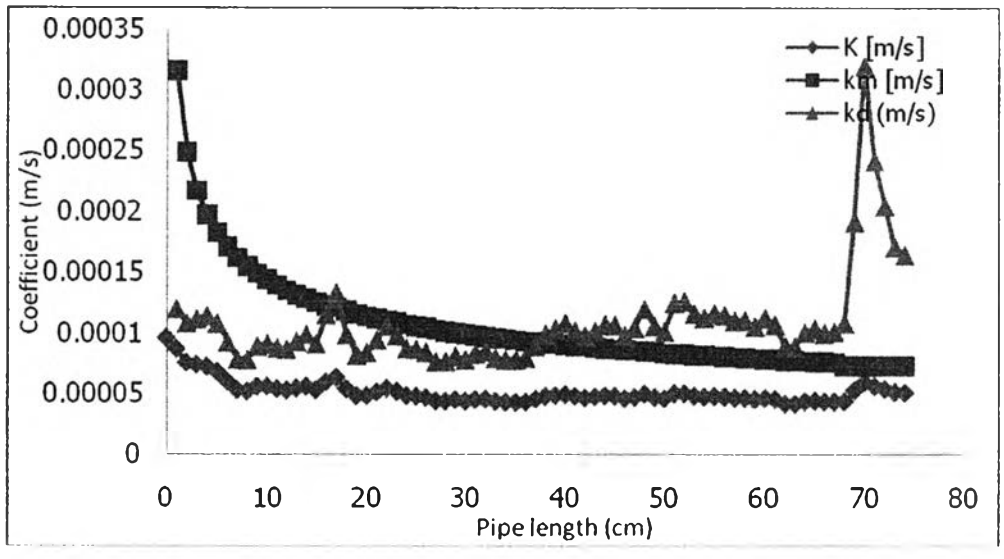

Figure C.5 The overall rate constant (K) and the dissolution coefficient (k_d) compared with the mass transfer coefficient (k_m) the pipe length under condition 0.21-0.25 mm, 100 defects/cm^3, 25°C and 25 LPM.

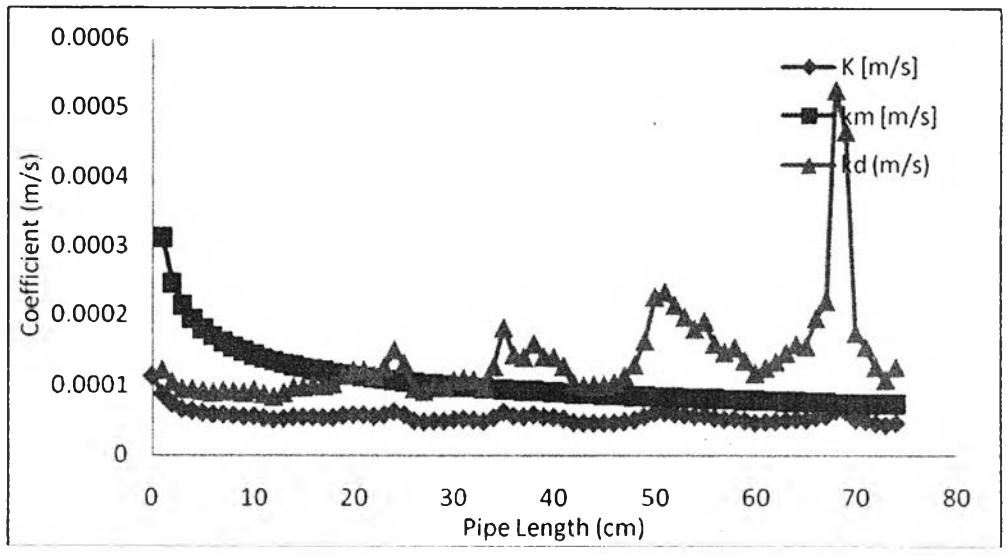

Figure C.6 The overall rate constant (K) and the dissolution coefficient (k_d) compared with the mass transfer coefficient (k_m) along the pipe length under condition 0.42-0.50 mm, 100 defects/cm^3, 25°C and 25 LPM.

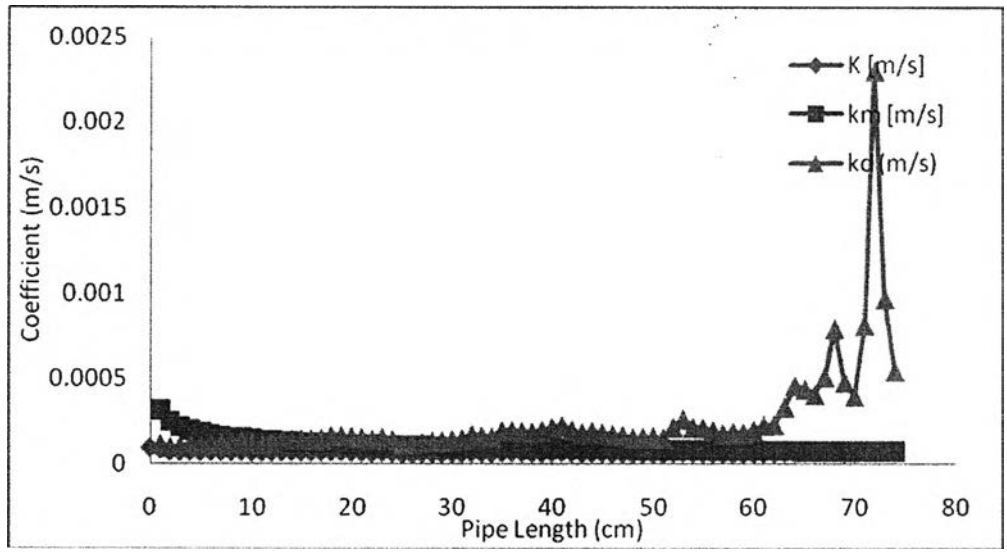

Figure C.7 The overall rate constant (K) and the dissolution coefficient (k_d) compared with the mass transfer coefficient (k_m) along the pipe length under condition 0.500-0.707 mm, 100 defects/cm^3, 25°C and 25 LPM.

C.3 Effect of Defect Concentration

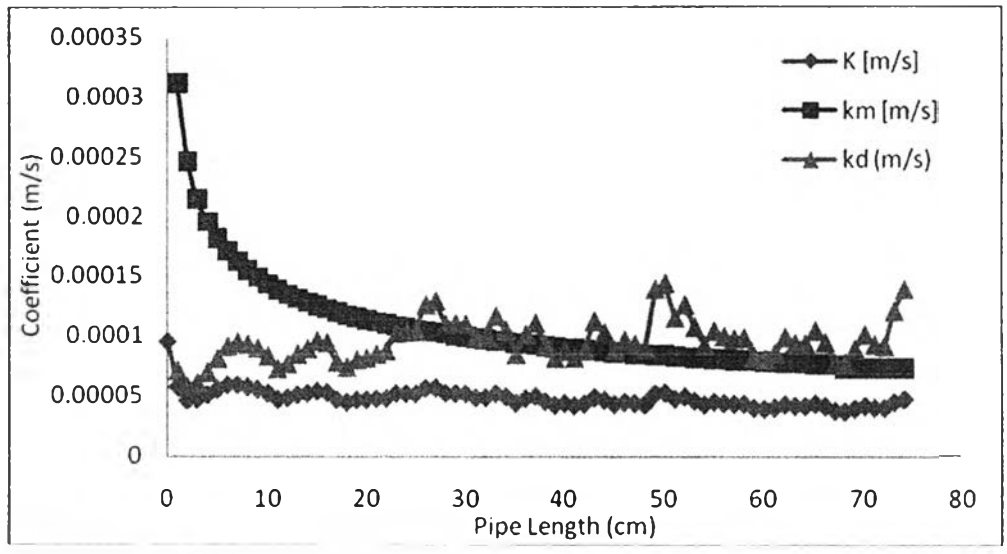

Figure C.8 The overall rate constant (K) and the dissolution coefficient (k_d) compared with the mass transfer coefficient (k_m) along the pipe length under condition 0.21-0.25 mm, 50 defects/cm^3, 25°C and 25 LPM.

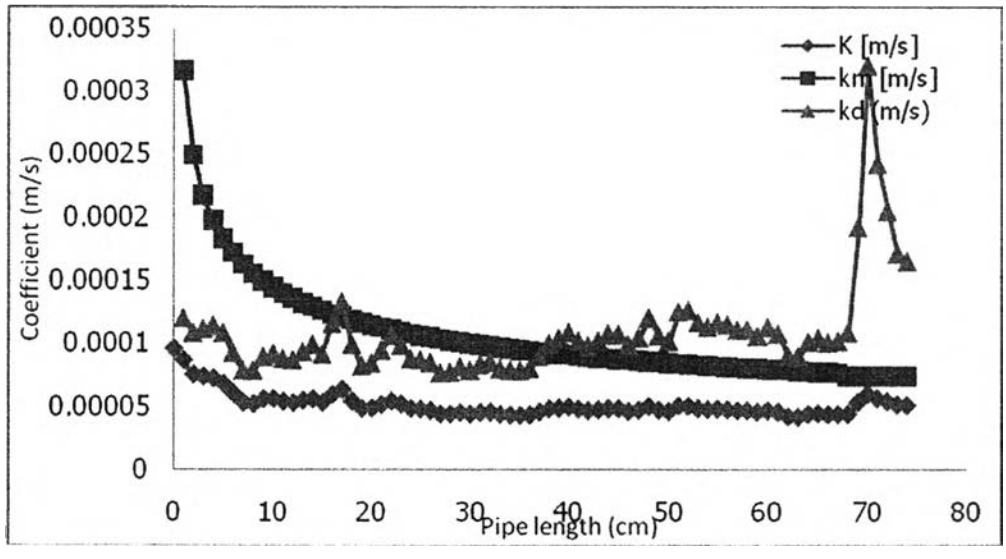

Figure C.9 The overall rate constant (K) and the dissolution coefficient (k_d) compared with the mass transfer coefficient (k_m) along the pipe length under condition 0.21-0.25 mm, 100 defects/cm^3, 25°C and 25 LPM.

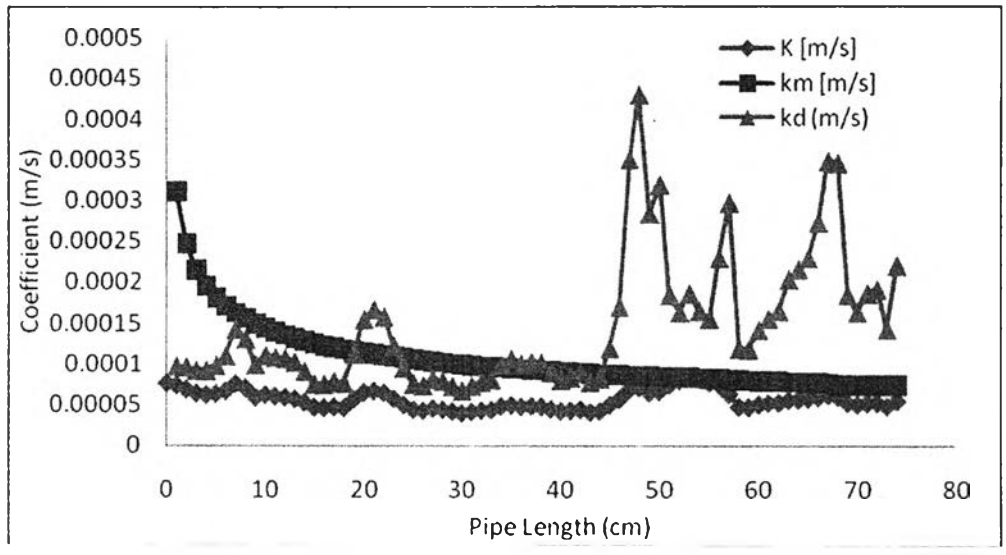

Figure C.10 The overall rate constant (K) and the dissolution coefficient (k_d) compared with the mass transfer coefficient (k_m) along the pipe length under condition 0.500-0.707 mm, 50 defects/cm^3, 25°C and 25 LPM.

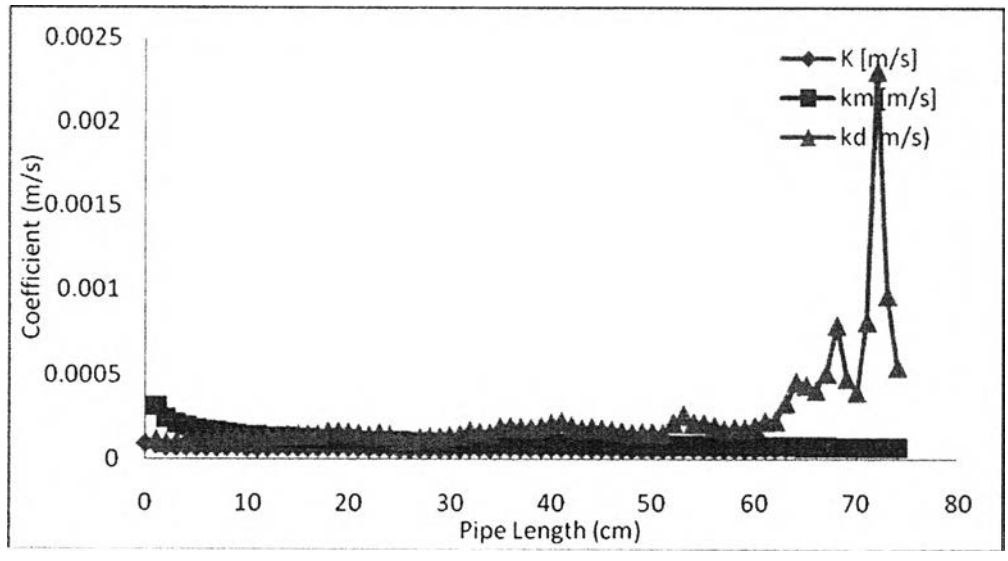

Figure C.11 The overall rate constant (K) and the dissolution coefficient (k_d) compared with the mass transfer coefficient (k_m) along the pipe length under condition 0.500-0.707 mm, 100 defects/cm^3, 25°C and 25 LPM.

C.4 Effect of Temperature

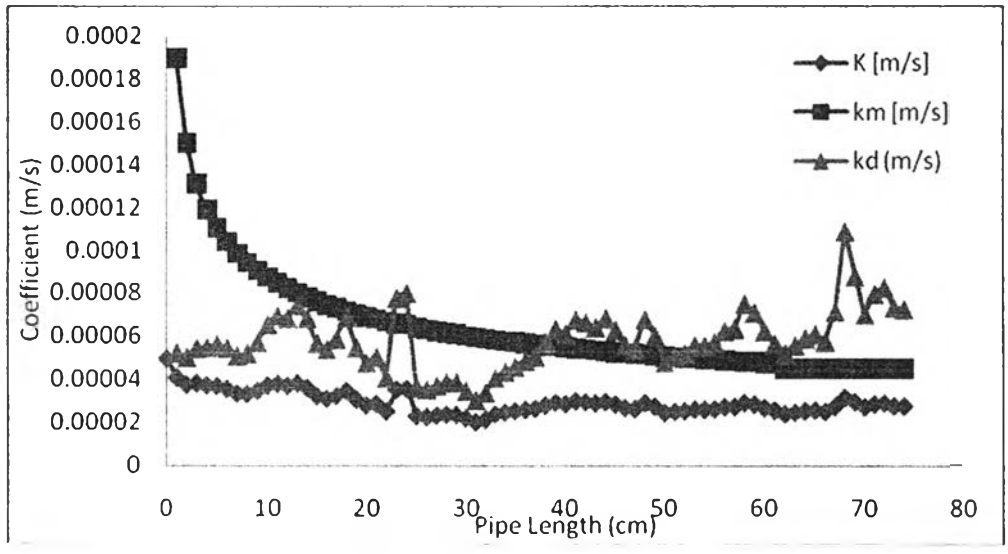

Figure C.12 The overall rate constant (K) and the dissolution coefficient (k_d) compared with the mass transfer coefficient (k_m) along the pipe length under condition pure plaster, 10°C and 25 LPM.

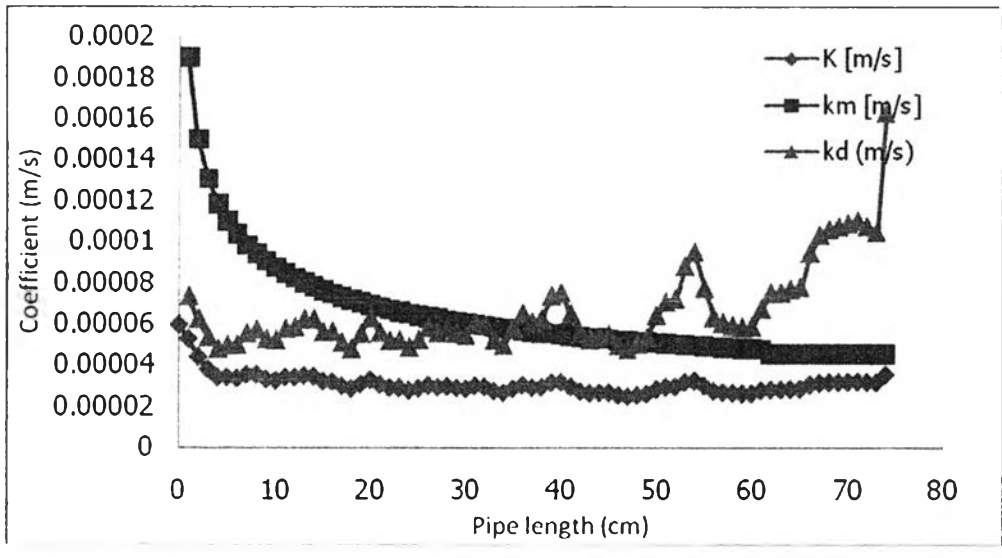

Figure C.13 The overall rate constant (K) and the dissolution coefficient (k_d) compared with the mass transfer coefficient (k_m) along the pipe length under condition 0.21-0.25 mm, 100 defects/cm^3, 10°C and 25 LPM.

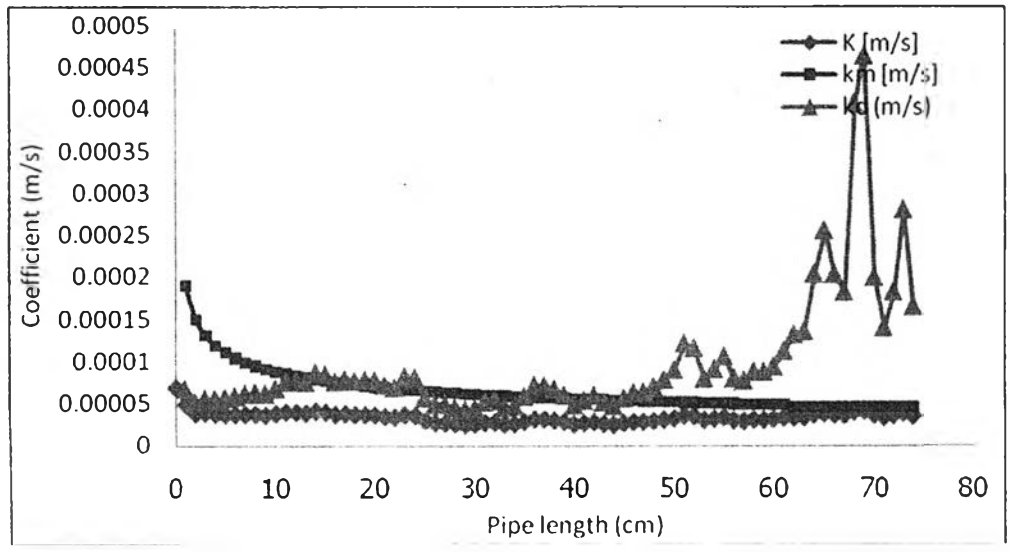

Figure C.14 The overall rate constant (K) and the dissolution coefficient (k_d) compared with the mass transfer coefficient (k_m) along the pipe length under condition 0.42-0.50 mm, 50 defects/cm^3, 10°C and 25 LPM.

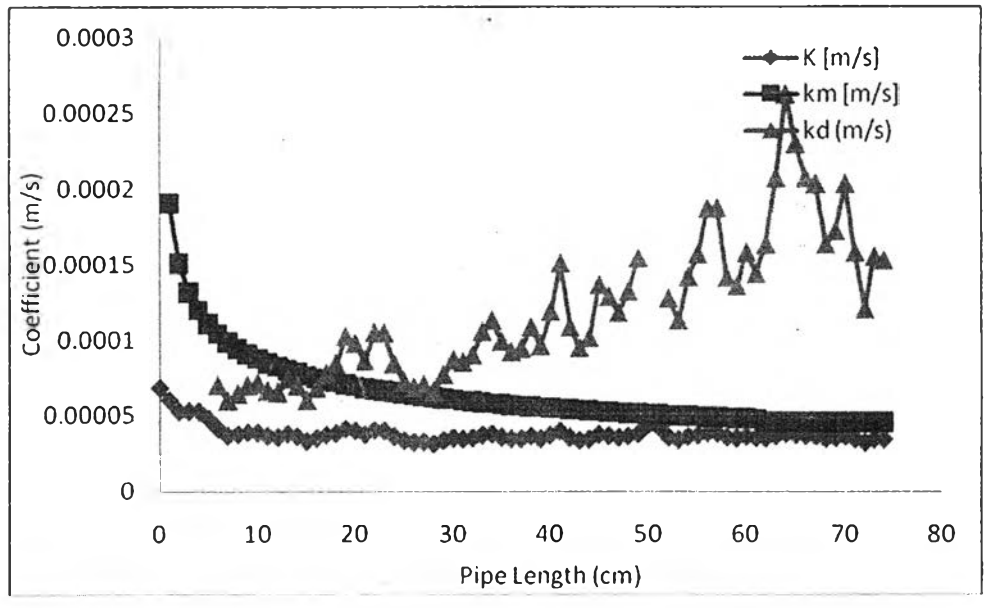

Figure C.15 The overall rate constant (K) and the dissolution coefficient (k_d) compared with the mass transfer coefficient (k_m) along the pipe length under condition 0.42-0.50 mm, 100 defects/cm^3, 10°C and 25 LPM.

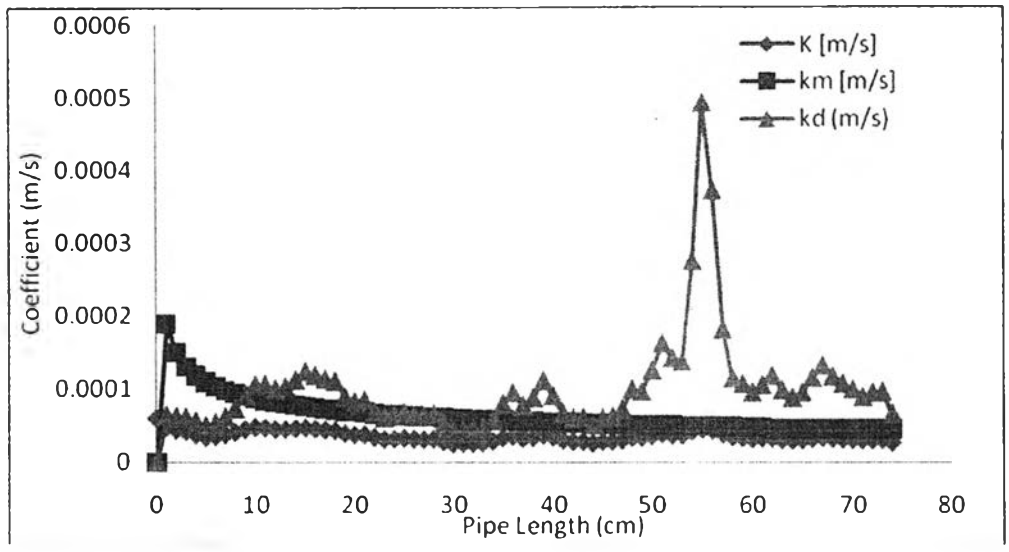

Figure C.16 The overall rate constant (K) and the dissolution coefficient (k_d) compared with the mass transfer coefficient (k_m) along the pipe length under condition 0.500-0.707 mm, 50 defects/cm^3, 10°C and 25 LPM.

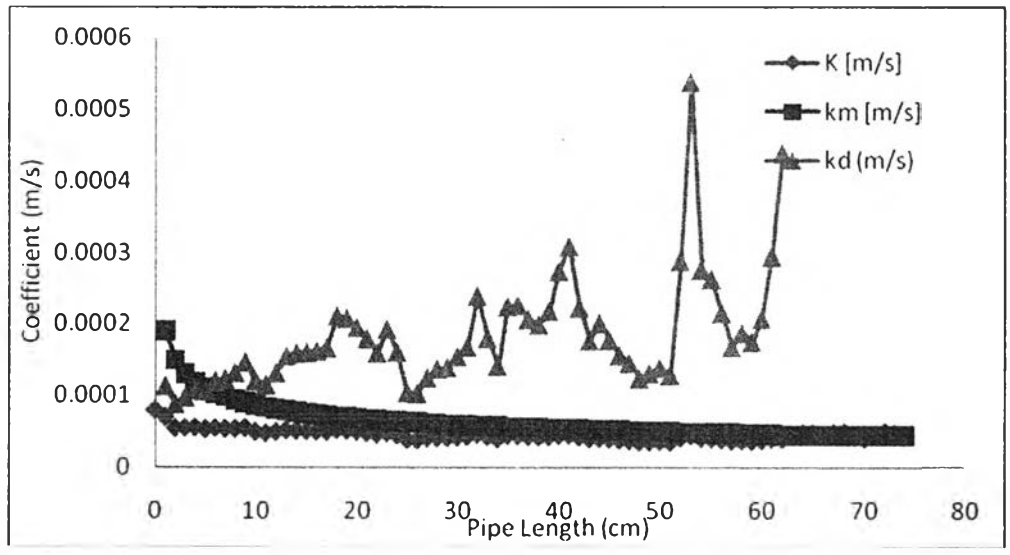

Figure C.17 The overall rate constant (K) and the dissolution coefficient (k_d) compared with the mass transfer coefficient (k_m) along the pipe length under condition 0.500-0.707 mm, 100 defects/cm^3, 10°C and 25 LPM.

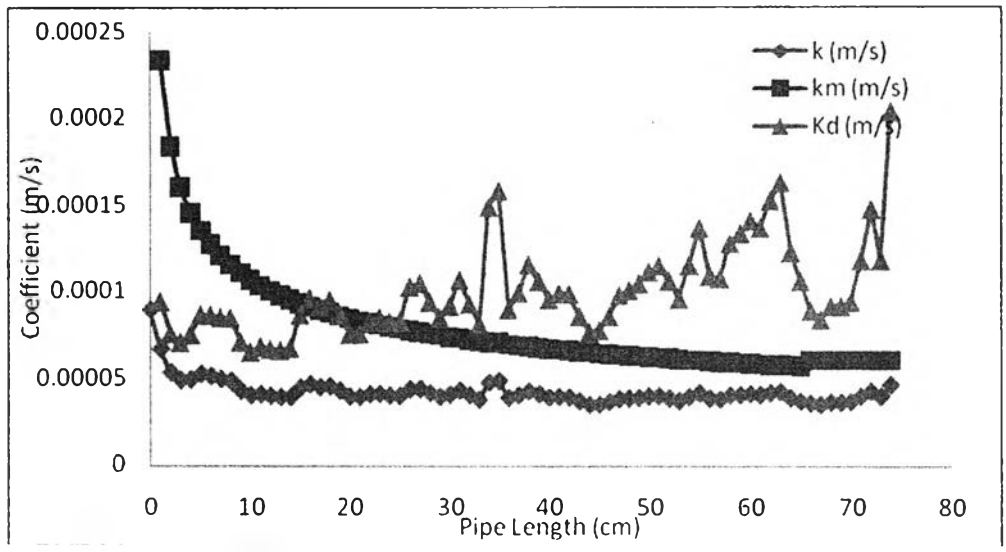

Figure C.18 The overall rate constant (K) and the dissolution coefficient (k_d) compared with the mass transfer coefficient (k_m) along the pipe length under condition pure plaster, 10°C and 35 LPM.

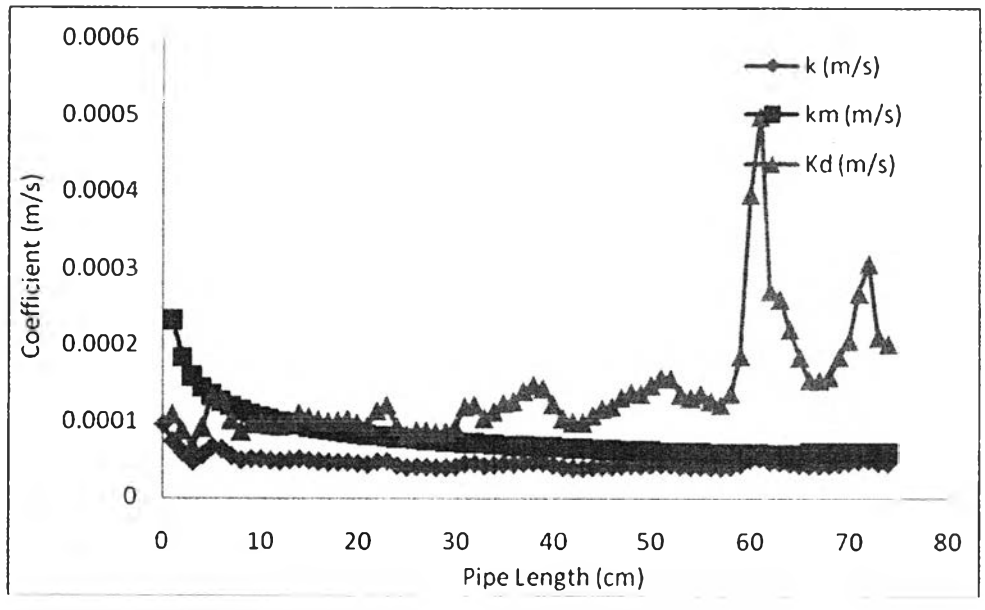

Figure C.19 The overall rate constant (K) and the dissolution coefficient (k_d) compared with the mass transfer coefficient (k_m) along the pipe length under condition 0.21-0.25 mm, 50 defects/cm^3, 10°C and 35 LPM.

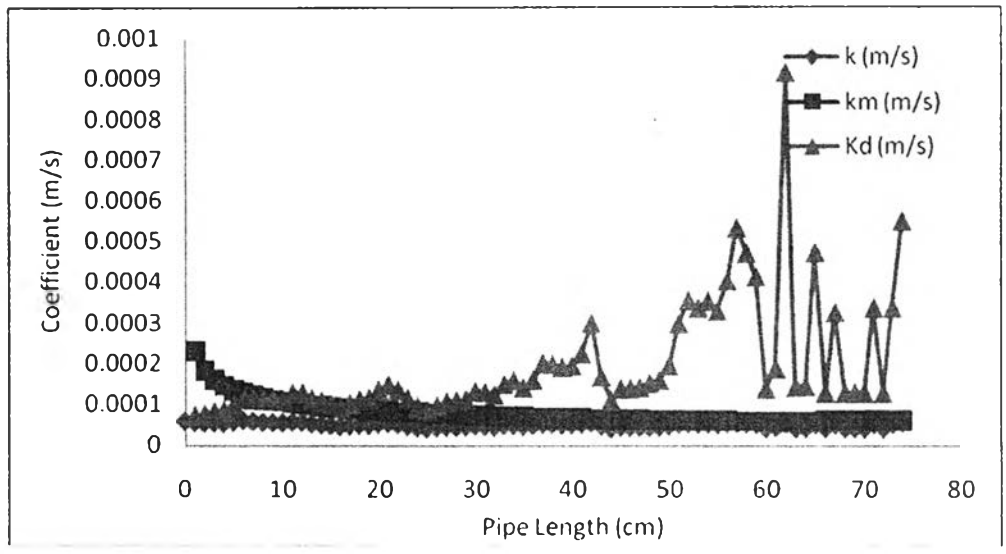

Figure C.20 The overall rate constant (K) and the dissolution coefficient (k_d) compared with the mass transfer coefficient (k_m) along the pipe length under condition 0.21-0.25 mm, 100 defects/cm^3, 10°C and 35 LPM.

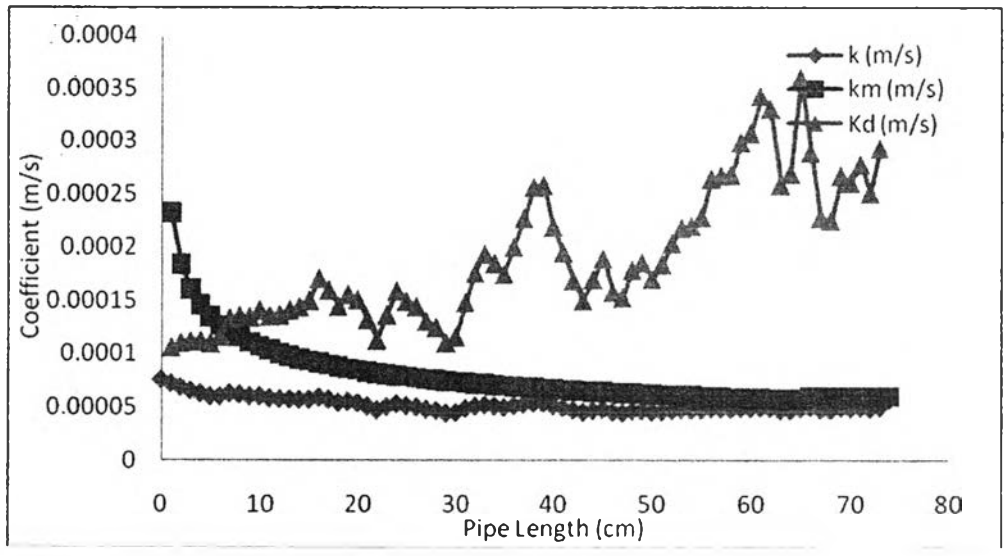

Figure C.21 The overall rate constant (K) and the dissolution coefficient (k_d) compared with the mass transfer coefficient (k_m) along the pipe length under condition 0.42-0.50 mm, 50 defects/cm^3, 10°C and 35 LPM.

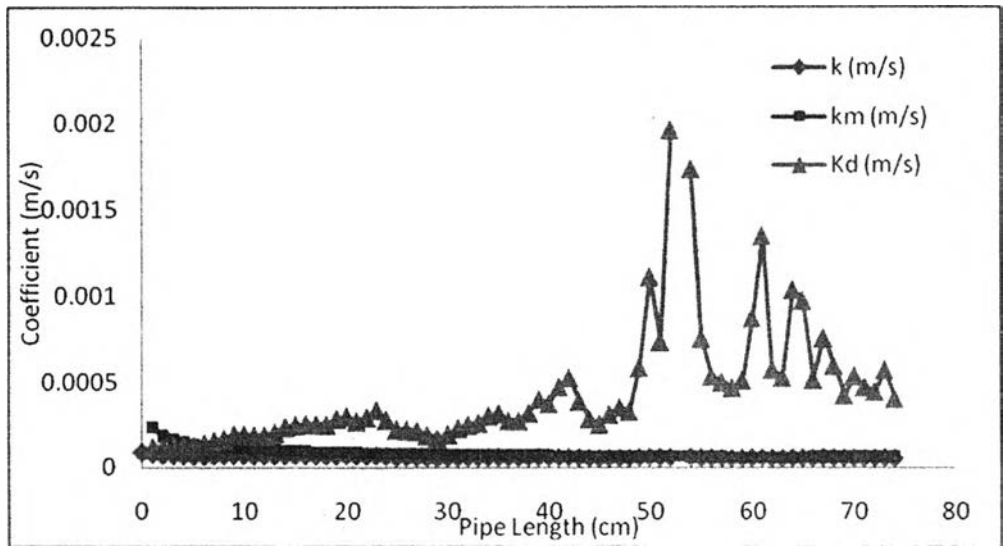

Figure C.22 The overall rate constant (K) and the dissolution coefficient (k_d) compared with the mass transfer coefficient (k_m) along the pipe length under condition 0.42-0.50 mm, 100 defects/cm^3, 10°C and 35LPM.

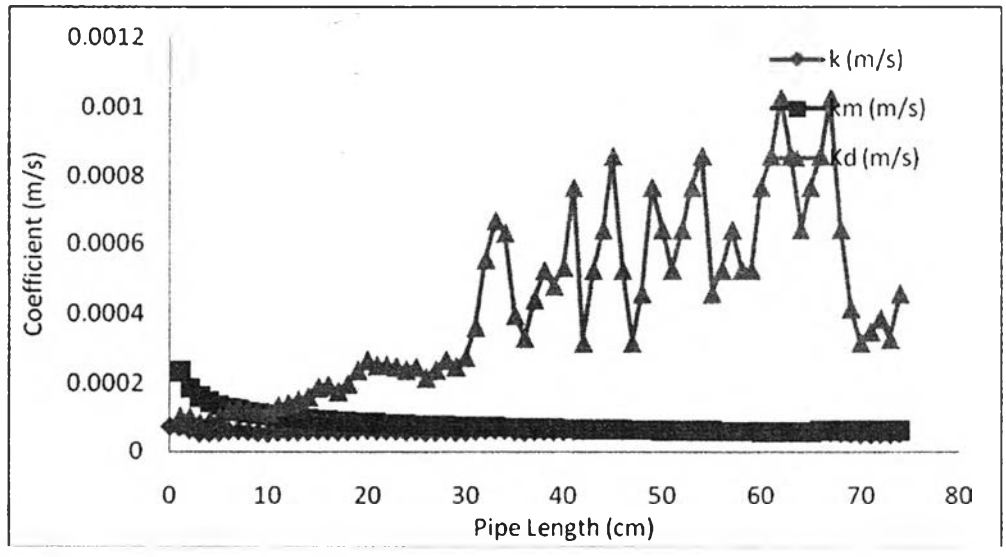

Figure C.23 The overall rate constant (K) and the dissolution coefficient (k_d) compared with the mass transfer coefficient (k_m) along the pipe length under condition 0.500-0.707 mm, 50 defects/cm^3, 10°C and 35LPM.

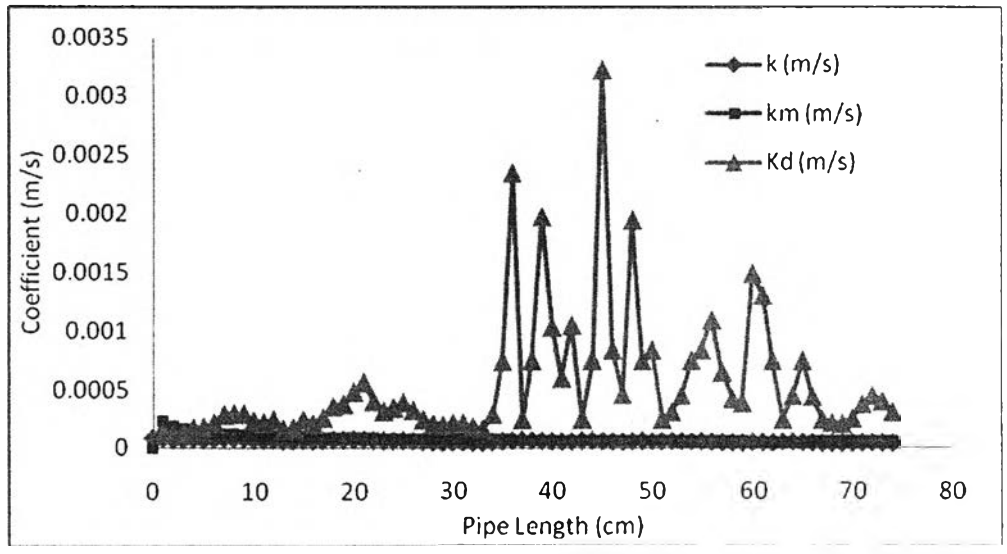

Figure C.24 Mass The overall rate constant (K) and the dissolution coefficient (k_d) compared with the mass transfer coefficient (k_m) along the pipe length under condition 0.500-0.707 mm, 100 defects/cm^3, 10°C and 35LPM

CURRICULUM VITAE

Name: Ms. Pasit Warunphaisal

Date of Birth: April 17, 1984

Nationality: Thai

University Education:

2002-2005 Bachelor Degree of Chemical Engineering, Faculty of Engineering, Thammasat University, Bangkok, Thailand

Working Experience:

2006-2007 Position: Process Engineer

Company name: HOYA LENS (Thailand) Co, ltd.

Proceedings:

Warunphaisal P., and Derek H. Lister (2009, April 22) Surface Dissolution and Formation of Scallops. Proceedings of 15th PPC Symposium on Petroleum, Petrochems, and Polymers, Bangkok, Thailand.

Presentations:

1. Warunphaisal P., and Rirksomboon T (2009, April 22) Surface Dissolution and Formation of Scallops. Poster presented at the 15th PPC Symposium on Petroleum, Petrochems, and Polymers, Bangkok, Thailand.